Central Metabolism Is Tuned to the Availability of Oxygen in Developing Melon Fruit

Kentaro Mori, Bertrand Beauvoit, Benoit Biais, Maxime Chabane, J. William Allwood, Catherine Deborde, Mickael Maucourt, Royston Goodacre, Cecile Cabasson, Annick Moing, et al.

frontiers in Plant Science

ORIGINAL RESEARCH
published: 15 May 2019
doi: 10.3389/fpls.2019.00594

Central Metabolism Is Tuned to the Availability of Oxygen in Developing Melon Fruit

*Kentaro Mori[1], Bertrand P. Beauvoit[1], Benoît Biais[1,2], Maxime Chabane[1], J. William Allwood[3], Catherine Deborde[1,2], Mickaël Maucourt[1,2], Royston Goodacre[4], Cécile Cabasson[1,2], Annick Moing[1,2], Dominique Rolin[1,2] and Yves Gibon[1,2]**

[1] UMR1332 BFP, INRA, Univ. Bordeaux, Villenave d'Ornon, France, [2] Plateforme Métabolome Bordeaux, MetaboHUB, Bordeaux Functional Genomic Centre, Villenave d'Ornon, France, [3] Environmental and Biochemical Sciences Group, The James Hutton Institute, Dundee, United Kingdom, [4] Manchester Institute of Biotechnology, University of Manchester, Manchester, United Kingdom

Respiration of bulky plant organs such as fleshy fruits depends on oxygen (O_2) availability and often decreases with O_2 concentration to avoid anoxia, but the relationship between O_2 diffusional resistance and metabolic adjustments remains unclear. Melon fruit (*Cucumis melo* L.) was used to study relationships between O_2 availability and metabolism in fleshy fruits. Enzyme activities, primary metabolites and O_2 partial pressure were quantified from the periphery to the inner fruit mesocarp, at three stages of development. Hypoxia was gradually established during fruit development, but there was no strong oxygen gradient between the outer- and the inner mesocarp. These trends were confirmed by a mathematical modeling approach combining O_2 diffusion equations and O_2 demand estimates of the mesocarp tissue. A multivariate analysis of metabolites, enzyme activities, O_2 demand and concentration reveals that metabolite gradients and enzyme capacities observed in melon fruits reflect continuous metabolic adjustments thus ensuring a timely maturation of the mesocarp. The present results suggest that the metabolic adjustments, especially the tuning of the capacity of cytochrome c oxidase (COX) to O_2-availability that occurs during growth development, contribute to optimizing the O_2-demand and avoiding the establishment of an O_2 gradient within the flesh.

Keywords: fruit, *Cucumis melo*, hypoxia, metabolism, modeling, cytochrome c oxidase

OPEN ACCESS

Edited by:
Alberto Battistelli, Italian National Research Council (CNR), Italy

Reviewed by:
Yi Shang, Yunnan Normal University, China
Marco Betti, University of Seville, Spain

****Correspondence:***
Yves Gibon
yves.gibon@inra.fr

Specialty section:
This article was submitted to Plant Metabolism and Chemodiversity, a section of the journal Frontiers in Plant Science

Received: *13 February 2019*
Accepted: *24 April 2019*
Published: *15 May 2019*

Citation:
Mori K, Beauvoit BP, Biais B, Chabane M, Allwood JW, Deborde C, Maucourt M, Goodacre R, Cabasson C, Moing A, Rolin D and Gibon Y (2019) Central Metabolism Is Tuned to the Availability of Oxygen in Developing Melon Fruit. Front. Plant Sci. 10:594. doi: 10.3389/fpls.2019.00594

INTRODUCTION

Bulky organs such as fruits, tubers or roots are prone to hypoxia and are known to decrease respiration with O_2 concentration to avoid anoxia (Geigenberger, 2003). Their respiration usually follows Michealis-Menten kinetics but the involved mechanisms are still unclear (Ho et al., 2011). There is also the widespread idea that bulky organs are characterized by up to strong O_2 gradients, as for example in potato tubers (Geigenberger, 2003). On the one hand, diffusional resistance in bulky organs has been invoked as explaining the occurrence of O_2 gradients, which result in limited availability of O_2 to respiration (Ho et al., 2011). On the other hand the recent finding of an O_2 sensor in Arabidopsis (Licausi et al., 2011) suggests that plant tissues are capable of metabolic adjustments limiting respiration, which occur well above the K_m value for O_2 of cytochrome c

oxidase (COX). Strikingly, whereas the K_m value of COX is often invoked in literature dealing with hypoxia, its capacity is rarely taken into account, although its modulation is a further and obvious control point for respiration. The picture is further complicated by the fact that hypoxia is actually needed in a range of processes associated to ripening. Thus, the production of a range of volatiles involves alcohol dehydrogenases (ADHs) and further component of fermentation (Manriquez et al., 2006). Due to its large size and easily accessible flesh, melon (*Cucumis melo* L.) is an interesting model to study relationships between oxygen availability and metabolism as influencing fruit growth and quality. Indeed, the balance between respiration and fermentation is at the heart of fruit development and the establishment of their quality during ripening (Pesis, 2005). Besides, melon is an economically important crop with an expanding world production situated around 32 million tons in 2012[1]. It is a member of the Cucurbitaceae family, which represents a yearly world market of hundreds of billions of dollars and 50 kg per person, with watermelon alone being the second most produced fruit in the world[1].

Whilst fruit flavor quality is largely the result of volatile compounds and their contribution to aroma, sweetness depends upon sugar concentration and the ratio between sugars and acids. Thus, melon fruits at commercial maturity are characterized by high contents of sucrose, glucose and fructose, as well as by a low organic acid content and the absence of starch (Lingle and Dunlap, 1987; Schaffer et al., 1987; Hubbard et al., 1989; Burger et al., 2000). The accumulation of these three soluble sugars appears to be controlled by carbohydrate metabolism in the fruit sink itself. Indeed, in the Curcubitaceae family, sucrose and the galactosyl-sucrose oligosaccharides, raffinose and stachyose, are synthetized in the leaf source and translocated to the fruit sink (Mitchell et al., 1992; Fiehn, 2003). Following which, raffinose and stachyose do not accumulate in the fruit, thus indicating a rapid metabolic conversion. Melon is a highly polymorphic species, in which variations in fruit sugar and acid contents are not just under genetic control, but are also influenced by the environment (Burger et al., 2000; Burger and Schaffer, 2007; Tang et al., 2012; Cohen et al., 2014). Numerous studies of fruit growth and ripening have shown that melon fruits undergo dramatic metabolic transitions. In particular, the accumulation of sucrose occurring at ripening has been associated with the loss of soluble acid invertase (AI) and a concomitant increase in sucrose phosphate synthase (SPS) (McCollum et al., 1988; Hubbard et al., 1989; Iwatsubo et al., 1992; Lester et al., 2001; Burger and Schaffer, 2007). However, both sucrose synthase (SuSy) and neutral invertase (NI) also show increased activities at ripening (Schaffer et al., 1987; Hubbard et al., 1989).

Recently, metabolomics approaches have been developed to identify key metabolites and their variations in fruits of various melon cultivars, including spatial and developmental measurements (Biais et al., 2009; Moing et al., 2011; Bernillon et al., 2013). Data analysis revealed several gradients of metabolites in fruit flesh at maturity such as sucrose, alanine, valine, γ-aminobutyric acid (GABA) and ethanol (Biais et al., 2010), which can be related with differences in metabolism. A decrease in the ATP/ADP ratio was also found to be associated with changes in alanine, GABA and ethanol, and was interpreted as being the result of acclimation to oxygen limitation as operated via alcoholic fermentation.

In the present study, metabolic changes occurring from the periphery to the fruit center and across three stages of fruit development were investigated using a multilevel approach. Thus major primary metabolites were determined by proton nuclear magnetic resonance spectroscopy (^{1}H NMR) and gas chromatography coupled to mass spectrometry (GC-EI-TOF/MS) to investigate how and when metabolic gradients take place during melon fruit development. Enzyme activities of sucrose metabolism, tricarboxylic acid (TCA) cycle and glycolysis were measured using robotized assays and a microplate-based assay for COX capacity was developed to investigate its involvement in fruit central metabolism. Oxygen partial pressure was measured by using an oxygen-sensitive optical glass-sensor and a model was built to calculate steady state O_2 concentrations at any position within the mesocarp based on O_2 diffusion and consumption. The calculation of O_2 demand using a construction cost model took in account the rates of biomass production at different depths within the mesocarp. By combining these approaches we investigated the relationship between O_2 diffusional resistance and metabolic adjustments occurring in melon fruit development.

MATERIALS AND METHODS

Melon Growth and Sample Handling

Melon plants (*Cucumis melo* L. var. Cantalupensis group Charentais cv. Escrito) were grown in an open field (9200 plants ha^{-1}) in Moissac (France, 44° 6′ 17″ N, 1° 5′ 6″ E) between April and August 2008 and Sainte-Livrade (France, 44° 23′ 56″ N, 0° 35′ 25″ E) between May and September 2011. Irrigation, fertilization and pathogen-pest control were performed according to standard commercial practices (Bernillon et al., 2013). Melon fruits were harvested at four stages of development (**Figure 1A**). Stage 1 corresponds to developing fruits with a diameter of 80 mm, Stage 2 to developing fruits with a diameter of 100–110 mm just before the appearance of the suberized net on the skin, Stage 3 to early ripening fruits with a fruit diameter of 130–135 mm and Stage 4 to ripening fruits at the beginning of abscission (commercial maturity). For O_2 tension measurements in melon mesocarp, 32 melons were harvested from Stages 1–3 and kept at laboratory temperature during the measurements. For ^{1}H-NMR analysis of polar compounds and enzyme assays, stages 2–4 were used. Nine melons were selected to make three homogeneous lots (biological replicates) of three fruits each. Two slices of 1 cm thickness were cut in the equatorial plane of each fruit. The skin and seeds were removed and five concentric mesocarp rings of flesh (7 ± 2 mm width) were taken from the periphery (outer mesocarp, named location 1) to the centre (inner mescocarp, named location 5) as explained in Biais et al. (2010) and **Figure 1B**. The flesh rings of a given position taken from a given fruit lot were pooled and

[1]http://faostat.fao.org/

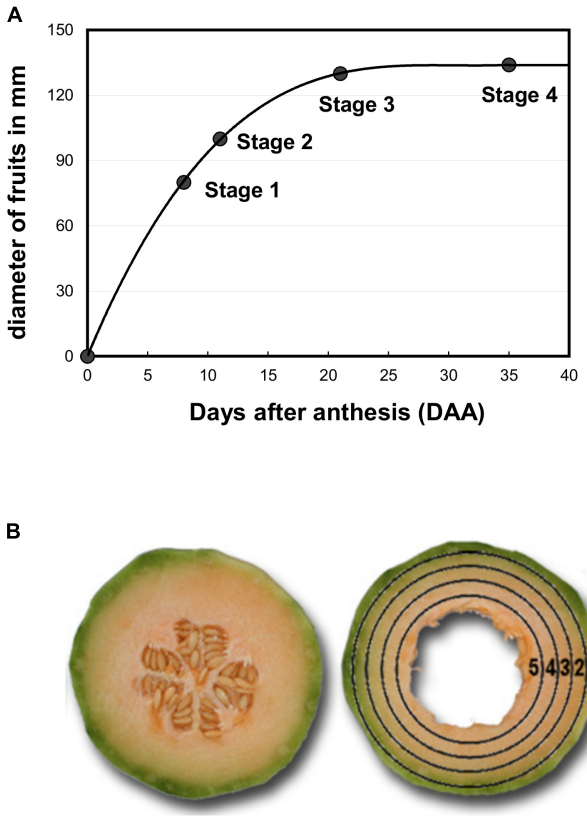

FIGURE 1 | (A) Growth curve of melon fruits (*Cucumis melo* L. var Cantalupensis group Charentais cv. Escrito). The diameter of harvested fruits was measured at each stage of development and was used to assess the growth curve. Melon fruits at stages 1, 2, 3, and 4 correspond to fruits harvested at 8, 11, 20, and 34 days after anthesis (DAA). **(B)** Sample preparation for biochemical analyses. A slice (7 ± 2 mm width) was first cut at the equator of the fruit. The seeds and placenta were removed, and then five concentric rings were cut in the slice and immediately frozen in liquid nitrogen. Position 1 corresponds to both the epicarp and green mesocarp, and positions 2–5 to the orange mesocarp.

immediately frozen in liquid nitrogen, before then being stored at −80°C. These were subsequently ground in liquid nitrogen and the 45 powdered samples (three stages × three biological replicates × five flesh positions) were further stored at -80°C until further processing. For ^{1}H-NMR analysis an aliquot of each sample was lyophilized. In parallel, dry matter content was determined using 250 mg FW powder aliquots dried in a 70°C oven.

Chemicals

All chemicals and substrates used for chemical and biochemical analyses were purchased from Sigma-Aldrich Ltd. (Gillingham, United Kingdom), except for acetyl coenzyme A, adenosine-5′-triphosphate (ATP), dithiothreitol, *n*-dodecyl β-D maltopyranoside, leupeptin, nicotinamide adenine dinucleotide (NAD), NADH, nicotinamide adenine dinucleotide phosphate (NADP), NADPH and phosphoenolpyruvate, that were purchased from Roche Applied Science (Meylan, F). All enzymes were purchased from Roche Applied Science (Meylan, F) except aldolase (from rabbit muscle), glycerokinase (from *E. coli*) and triose phosphate isomerase (from rabbit muscle) that were purchased from Sigma-Aldrich Ltd. (Gillingham, United Kingdom). Bradford reagent was purchased from Bio-Rad (Marnes-la-Coquette, F). Reagents used for mRNA quantification were purchased from Fisher Scientific (Illkirch, F), Qiagen (Courtaboeuf, F), Bio-Rad (Mitry-Mory, F), and Promega (Charbonnières-les-Bains, F).

^{1}H NMR and GC-EI-TOF/MS Analyses of Polar Metabolites of Ground Flesh Samples

Polar metabolites were extracted from ground melon samples corresponding to the five concentric mesocarp rings of flesh. For NMR analyses the frozen powdered samples were lyophilized and polar metabolites were extracted from 50 mg of lyophilized powder successively with 2 ml of ethanol/water mixtures: 80/20, 50/50 (v/v) and pure water (4 ml) for 15 min at 80°C. The supernatants were combined, dried under vacuum and lyophilized. The pellet was kept for the determination of protein content. Two technical replicates were prepared per biological sample. The lyophilized extracts were mixed with 500 µl of 400 mM potassium phosphate buffer solution pH 6.0, 1 mM ethylene diamine tetraacetic acid disodium salt (EDTA), in D_2O. The pH was the adjusted to 6 with KOD when necessary, and lyophilized again. The lyophilized extracts were stored in darkness under vacuum at room temperature, before ^{1}H-NMR analysis which was completed within 1 week. For ^{1}H-NMR analysis, each dried pH-adjusted extract was solubilized in 0.5 ml of D_2O with (trimethylsilyl) propionic-2,2,3,3-d4 acid (TSP) sodium salt (0.01% final concentration for chemical shift calibration), centrifuged at 10,000 g for 5 min and transferred into an 5 mm NMR tube. Quantitative ^{1}H-NMR spectra were recorded at 500.162 MHz and 300 K on a Bruker Avance spectrometer (Wissembourg, France), using a 5 mm inverse probe and an electronic reference for quantification as described previously (Mounet et al., 2007; Biais et al., 2009; Moing et al., 2011). For GC-EI-TOF/MS, 100 mg aliquots (± 2 mg) of frozen ground samples were extracted with 1 ml chloroform/methanol/water (1:2.5:1), the polar metabolite fraction was obtained by further addition of 0.5 ml of water and dried by speed vacuum concentration. The extracts were derivatized and analyzed by GC-EI-TOF/MS on an Agilent 6890N gas chromatograph (Stockport, United Kingdom), coupled to a Leco Pegasus III mass spectrometer (St Joseph, United States). Chromatographic deconvolution was performed within the LECO ChromaTof v2.15 software, the extracted peak areas for each of the deconvolved metabolite features were normalized against the succinic-*d4* acid internal standard. The detailed procedures for extraction, derivatization, sample analysis, mass spectral deconvolution and metabolite identification, have been described in detail previously (Allwood et al., 2009; Biais et al., 2009; Moing et al., 2011). The full dataset can be found at http://www.cbib.u-bordeaux2.fr/MERYB/public/PublicREF.php?REF=M08002.

Protein Content

The pellet was resuspended in 1 ml 100 mM NaOH and heated for 30 min at 95°C. After cooling to room temperature and centrifugation at 5,000 g, the protein content of the remaining supernatant was determined according to Bradford (1976).

Enzyme Activity Measurements

Aliquots of 50 mg fresh weight (FW) were extracted by vigorous shaking with 500 µl of extraction buffer composed of 20% (v/v) glycerol, 0.25% (w/v) bovine serum albumin, 1% (v/v) Triton-X100, 50 mM HEPES/KOH pH 7.5, 10 mM $MgCl_2$, 1 mM EDTA, 1 mM EGTA, 1 mM ε-aminocaproic acid, 1 mM benzamidine, 10 mM leupeptin, 0.5 mM dithiothreitol, and 1 mM phenylmethylsulfonylfluoride, which was added just prior to extraction. The following enzyme activities (SPS, SUSY, acid invertase, PFP, PFK, MDH, PK, PEPC, CS, IDH, see **Figure 3** legend for the full enzyme name) were assayed using a robotized platform as described in Gibon et al. (2004, 2006, 2009), Studart-Guimaräes et al. (2005), and Steinhauser et al. (2010).

Enolase was assayed in the direction of phospho*enol*pyruvate production as described previously (Burell et al., 1994). The assay consisted of 10 µl desalted extract in 100 mM HEPES/NaOH (pH 7.5), 10 mM $MgCl_2$, 0.2 mM NADH, 2.7 mM ADP, 5 units.ml^{-1} pyruvate kinase and 6 units.ml^{-1} lactate dehydrogenase. The reaction was initiated by the addition of 2-phosphoglycerate to a final concentration of 0.5 mM.

NADP dependent malic enzyme activity (NADP-ME) was assayed using a protocol adapted from Wheeler et al. (2005). The assay was performed with 2 µl of extract in 100 mM HEPES/KOH (pH 7.5), 10 mM $MgCl_2$, 1 mM $NADP^+$ and 0.05% (v/v) Triton X100. The reaction was initiated by addition of malate to a final concentration of 10 mM and a final volume of 20 µl. After 40 min of incubation at 25°C, the reaction was stopped by the addition of 20 µl of HCl 0.5 M/Tricine/KOH 0.1 M (pH 9). Following sample mixing and a 10 min delay, the acid was neutralized by the addition of 20 µl of 0.5 M NaOH. The quantification of phospho*enol*pyruvate was then performed by adding 100 mM HEPES/KOH (pH 7.5), 10 mM $MgCl_2$, 0.05% (v/v) Triton X100 and 1 mM NADH in a final volume of 110 µl. Absorbance at 340 nm was recorded until stabilized, then 2 µl of lactate dehydrogenase 100 units.ml^{-1} were added to start the reaction and absorbance was again recorded until stabilized.

Alcohol dehydrogenase (ADH) activity was assayed using 5 µl of extract in 100 mM HEPES/KOH (pH 7.5), 0.1 mM EDTA, 1.2 mM NAD^+, 1 mM thiazolyl blue tetrazolium bromide (MTT), 0.2 mM phenazine ethosulfate and 0.05% (v/v) Triton X100. The reaction was initiated by the addition of ethanol to a final concentration of 25 mM and a final volume of 100 µl. Absorbance was read at 600 nm until rate stabilized.

The respiratory chain enzymes, i.e., cytochrome *c* oxidase (COX) and succinate dehydrogenase (SDH), were assayed as described in Rustin et al. (1994) and Vinogradov et al. (1980), respectively, using a modified extraction procedure adapted to plant tissues. Briefly, aliquots of 100 mg FW powder were extracted at 4°C by vortexing with 500 µL of potassium phosphate buffer solution (50 mM potassium phosphate pH 7.2, 1 mM EDTA) supplemented with 1% (w/v) *n*-dodecyl β-D maltopyranoside. To eliminate low molecular weight reducing compounds and to decrease the detergent concentration, the homogenate was subsequently filtrated through a 2 ml column of Sephadex G25 coarse medium (Sigma-Aldrich, Lyon, France), equilibrated at 4°C with the phosphate buffer solution supplemented with 0.1% (w/v) *n*-dodecyl β-D maltopyranoside. Sephadex columns were then centrifuged at 4°C for 2 min at 2400 *g* and the filtrate stored on ice. The enzyme recovery was checked using isolated mitochondria for which COX and SDH activities can be measured before and after filtration. SDH was assayed at 25°C using the phenazine methosulfate-(PMS) mediated reduction of dichloroindolphosphate (DCIP) monitored at 600 nm with a spectrophotometer. The SDH assay consisted of 10–50 µL of filtrate in a final volume of 1 ml of phosphate buffer solution (pH 7.2) containing 0.1% (w/v) *n*-dodecyl β-D maltopyranoside, 5 mM succinate, 0.1 mM KCN and 0.05 mM DCIP. The reaction was initiated by the addition of PMS to a final concentration of 1.6 mM. COX was assayed at 25°C by monitoring the oxidation of reduced cytochrome *c* at 550 nm. The COX assay consisted of 10–50 µL of filtrate in a final volume of 1 ml of phosphate buffer solution (pH 7.2) containing 0.1% (w/v) *n*-dodecyl β-D maltopyranoside. The reaction was initiated by the addition of chemically-reduced cytochrome *c* at a final concentration of 50 µM. The specificity of the assay was checked by addition of KCN.

O_2 Measurements Within the Melon Mesocarp

The O_2 tension (expressed in kPa) was measured by using an oxygen-sensitive optical glass-sensor (microsensor, PreSens, Neuburg, DE) connected to a fiber optic oxygen meter (MicroX TX3 PreSens, Neuburg, DE), and was based upon dynamic fluorescence quenching. The O_2 microprobe tip has a diameter of 140 µm and is protected by a hypodermic needle linked to a syringe. In contrast to oxygen microelectrodes, this oxygen microprobe does not consume oxygen and shows no stirring dependence of the signal, and thus prevents the establishment of an artificial oxygen sink within the measured tissue. The microsensor was calibrated in water that had been well equilibrated with ambient air (21 kPa O_2) and also in water that had been depleted of oxygen with Na_2SO_3. The electrode signal was stable for at least 4 h. The fruit was first placed on a support and fixed. Subsequently, the microsensor was positioned on the fruit surface and driven into the fruit by a micromanipulator at 5 mm intervals. Just after the insertion of the needle, the microsensor occupied the small hole in the tissue at the needles entry point, without being in contact with the outside. At each position the sensor was paused for approximately 120 s to allow equilibration and to obtain a continuous measurement. The mean of 100 measurements with a standard error of less than 5% represents a single data point in the subsequently presented figures. From 32 melons harvested at stages 1–4, 16 were used within 48 h to measure O_2 tension at three different depths (7.5, 12.5, and 17.5 mm) in the mesocarp and at three different equatorial positions. Only in mature fruits (stage 4), the O_2

tension was measured deeper into the mesocarp (22.5, 27.5, and 32.5 mm). After the measurements were performed, the melon fruits were sliced at the level of the measurement transect to verify the exact position of the sensor tip within the distinct zones of the mesocarp.

Modeling of the Oxygen Gradient Within the Melon Mesocarp

The oxygen concentration within the melon was modeled assuming that the steady state oxygen concentration at any position within the mesocarp is a function of the oxygen diffusion and consumption within the tissue. This was achieved by solving the time-dependent diffusion equation in spherical co-ordinates with spherical symmetry (McElwain, 1978):

$$\frac{\partial C}{\partial t} = D\left(\frac{\partial^2 C}{\partial R^2} + \frac{2}{R}\frac{\partial C}{\partial R} - \frac{\alpha C}{C + K_\mathrm{m}}\right)$$

with the following dimension-less variables:

$$C = \frac{P}{P_0}\ ;\quad R = \frac{r}{r_0}\ ;\ \alpha = \frac{V_{\mathrm{oxygen}} r_0^2}{P_0 D};\ K_\mathrm{m} = \frac{k_\mathrm{m}}{P_0}$$

Where: R is the relative distance from the centre, r_0, the radius of the melon, D, the diffusion coefficient within the mesocarp ($D = 2.4\ 10^{-5}$ cm^2 s^{-1}) and P_0, the oxygen tension outside the melon (21 kPa, at 25°C). K_m is the half saturation constant of the terminal oxidase of the respiratory chain. It was equal to either 0.108 or 0.134 kPa, for the COX or the alternative oxidase, respectively (Armstrong and Beckett, 2011). These values were assumed to be constant as a function of the depth (i.e., as a function of the respiratory rate). V_{oxygen} is the O_2 consumption rate of the tissue, which was estimated using a construction cost model (see below) and was computed as a depth-dependent polynomial function (see **Supplemental Figures S1**, **S2**).

The steady state problem ($\partial C/\partial t = 0$) was solved using the PDEX4 function in Matlab 2007 and the following initial and boundary conditions:

at $t = 0$, $C = 0$

at $r = 0.5\ r_0$, $\frac{dC}{dR} = 0$

at $r = r_0$, $\frac{dC}{dR} = \frac{hr_0}{D}(1 - C)$

where h is the permeability coefficient of the melon skin, expressed in cm s^{-1}.

The Matlab script is provided within the **Supplementary Material** (Note 1 in **Supplemental Data**).

For each developmental stage, an h-value was obtained by fitting the O_2 measurements and minimizing an *Obj* score, i.e., the sum of the squared residuals weighed by the standard deviation of each measurement, according to the following equation:

$$Obj = \sum_{\mathrm{i}=1}^{n}\left(\frac{[\mathrm{O_2}]_\mathrm{i}\, cal - [\mathrm{O_2}]_\mathrm{i}\, exp}{\sigma_\mathrm{i} exp}\right)^2$$

where n is the number of depths, $[O_2]_\mathrm{i}cal$, and $[O_2]_\mathrm{i}exp$, the calculated and experimental values of O_2 concentration at a given depth and $\sigma_\mathrm{i}exp$, the standard deviation of the measures.

Calculation of the Oxygen Demand Using a Construction Cost Model

Rates of biomass production at different depths within the mesocarp were calculated by expressing biomass as a function of time for five layers of equal thickness. For this, considering that the fruit is a sphere, the volumes of the six corresponding layers nested into one another's spheres, were calculated throughout development, based on estimates of the changes in fruit diameter, and subtracted to obtain the volumes of the sectors (see **Supplemental Figures S1**, **S2**). Volumes were then converted to biomass using density estimates and fitted polynomials that were integrated to obtain the rates of biomass production.

The flux of oxygen consumption was calculated at each stage and for each sector as the sum of the growth-linked and maintenance respiration, according to the following equation (Heuvelink, 1995; Liu et al., 2007):

$$\frac{dC_{\mathrm{respiration}}}{dt} = q_{\mathrm{growth}} * \frac{dDW}{dt} + q_{\mathrm{maintenance}} * DW * Q_{10}^{(t^\circ - 20)/10} \quad (1)$$

where: $dC_{\mathrm{respiration}}/dt$ is the respiration-linked carbon consumption of the sector (g of C day^{-1} g^{-1} DW); dDW/dt and DW, the growth rate and the dry weight content of the sector, respectively, Q_{10}, the temperature-dependent coefficient for maintenance respiration (Q_{10} = 2) and t°, the growth temperature (averaged temperature of the culture was 25.4°C). q_{growth}, the carbon requirement for growth-linked respiration, is well known for a variety of fleshy fruits and is equal to 0.1 g C g^{-1} DW at 20°C (Heuvelink, 1995; Liu et al., 2007; Dai et al., 2010, and references therein). In contrast, $q_{\mathrm{maintenance}}$, the carbon requirement for cell maintenance, is hardly available for fruits and needs to be estimated. It was calculated assuming that the maintenance-linked respiration of aerobically grown cells is proportional to the amount of respiratory complexes and accounts for 10–20% of the complex IV (i.e., COX) activity (Devin et al., 2006, and references therein). Finally, the oxygen consumption rate (expressed in µmol O_2 min^{-1}.ml^{-1}) was calculated by using the sector volume, the fresh-to-dry weight ratio, assuming that the tissue density is equal to 1 g FW per ml and considering that the coefficient of respiration equals 1, i.e., neglecting the ethanol production vs. oxidative phosphorylation.

Total RNA Extraction and qRT-PCR Analysis

Total RNA was extracted from melon mesocarp tissues using Trizol reagent (Fisher scientific). One hundred milligrams of frozen mesocarp powder were homogenized with 1 ml of Trizol reagent and spiked with a mix of the five artificial poly(A+) RNAs (ArrayControl$^{\mathrm{TM}}$ Spots and Spikes, Fisher Scientific) to achieve absolute quantification of transcripts. Concentration of RNA spikes were 2.4×10^{11}, 4.8×10^{10}, 2.4×10^{9}, 2.5×10^{7}, and 4.0×10^{6} copies per gram FW. Total RNA was purified with the RNeasy kit (Qiagen), then treated with the Turbo DNase

(Fisher Scientific). cDNA was synthesized from 500 ng total RNA using the iScript cDNA synthesis kit (Bio-Rad) and was diluted 5 times with nuclease free water. qRT-PCR reactions and data analysis were performed as described by Piques et al. (2009) with slight modifications. The 20 µl PCR mixture contained 2 µl of the diluted cDNA template, 10 µl of 2 × GoTaq® qPCR Master Mix (Promega), and 0.2 µM of the forward and reverse primers for each gene. The primers used to amplify melon genes were designed using primer3 software[2]. The primers for the RNA spike-in controls were designed as described in Pyl et al. (2012). All primer sequences are available in **Supplemental Table S2**. PCR reactions were run on the CFX96™ Real-Time PCR Detection System (Bio-Rad) under the following conditions: 95°C for 2 min, followed by 40 cycles at 95°C for 3 s, at the annealing temperature of 60°C for 30 s, and a dissociation curve analysis, 65–95°C with temperature increment of 0.5°C every 5 s. For each sample, cycle threshold values and copy numbers for the 5 spike-in controls were used to generate a standard curve. All standard curves, derived from the five spike-in controls, had R^2-values higher than 0.99 and were used to calculate the concentration of the mRNA as copy number g^{-1} FW and copy number mg^{-1} protein.

Statistical Analysis

Principal component analysis (PCA) and correlation analysis (Pearson coefficient) were performed using R[3] with the package FactomineR (Lê et al., 2008).

RESULTS

Melon fruits (*Cucumis melo* var. Cantalupensis group Charentais cv. Escrito) were grown in the open field under common agricultural practices; the fruits were ripe within 45 days post anthesis. The Escrito cultivar, which is widely cultivated in France, is considered as average regarding aromaticity and shelf-life (Allwood et al., 2014). To study the metabolic changes that occur during ripening, samples were taken during fruit growth (stage 2), at early fruit ripening (stage 3) and at fruit maturity (stage 4) (**Figure 1A**). For each stage, nine fruits were harvested and cut into five concentric mesocarp rings, the concentric tissue sections were pooled for three fruits and homogenized, thus creating three replicate samples each made up of three pooled fruits, prior to extraction and metabolite quantification (**Figure 1B**). For oxygen pressure measurements, an additional stage corresponding to fruit growth (stage 1) was used because data obtained at stage 2 appeared more scattered than at stages 3 and 4.

Maturation of the Melon Mesocarp Is Centrifugal

The changes in metabolites that occurred during fruit development in the five concentric mesocarp rings of flesh taken from the periphery (outer mesocarp, sector 1) to the centre (inner mesocarp, sector 5) are presented in **Figure 2** (see also **Supplemental Table S1**). Soluble sugars were the most abundant metabolites throughout fruit development. Whilst sugars such as stachyose and galactose exhibited a steady and very low content in the fleshy mesocarp at the three development stages (0.15 and 0.5 $\mu mol.g^{-1}$ FW, respectively), Suc, glucose (Glc), and fructose (Fru) (the major soluble sugars in melon) revealed different patterns. Suc exhibited a steady and relatively low content in the fleshy mesocarp around 20–40 $\mu mol.g^{-1}$ FW during fruit development (stage 2) and early fruit ripening (stage 3), whilst at fruit maturity (stage 4) a strong Suc gradient was observed from the periphery to the center of the fruit. Suc concentration increased regularly from the periphery (50 $\mu mol.g^{-1}$ FW, position 1) to the center of the fruit (200 $\mu mol.g^{-1}$ FW, position 5). In contrast, Glc and Fru concentrations were highest during fruit development, ranging between 80 and 110 $\mu mol.g^{-1}$ FW at stages 2 and 3 and decreased at fruit maturity (stage 4), with 60 and 80 $\mu mol.g^{-1}$ FW for Glc and Fru, respectively. The two hexoses exhibited a small gradient between outer and inner mesocarp at stages 2 and 3. The Glc and Fru concentrations increased regularly from the periphery (80 $\mu mol.g^{-1}$ FW, position 1) to the center of the fruit (110 $\mu mol.g^{-1}$ FW, position 4 and 5). At maturity the Glc gradient disappeared and the Fru gradient was inverted.

Among the five detected organic acids, pyruvate, fumarate and succinate showed the same pattern. During fruit development (stage 2) and at the early ripening stage (stage 3), they were almost undetectable, but increased dramatically at fruit maturity, where a marked gradient was also observed from the periphery to the center of the fruit. Malate and citrate had different patterns. With the exception of the outer mesocarp (position 1), malate levels remained low and stable throughout the rest of the fleshy mesocarp (less than 5 $\mu mol.g^{-1}$ FW), whilst a small gradient was apparent for citrate between the outer and inner mesocarp (15–20 $\mu mol.g^{-1}$ FW) during stages 2 and 3. At maturity, the citrate gradient was still apparent in the fleshy sectors, with slightly higher concentrations (20–25 $\mu mol.g^{-1}$ FW) than observed during the earlier developmental stages, further a strong increase of citrate was observed in the peripheral sector at full maturity.

Eleven and nine amino acids were measured by GC-EI-TOF/MS and ^{1}H-NMR, respectively. Among the eight major amino acids observed (**Figure 2**), five were found at concentrations greater than 2 $\mu mol.g^{-1}$ FW in the fleshy mesocarp at maturity (Ala, Gln, Glu, Asp, and GABA). All these amino acids, as well as the three aromatic amino acids, showed the same pattern of accumulation. Whilst no strong gradients were observed for amino acids during development, marked gradients were observed from the periphery to the center of the fruit for almost all amino acids measured at full maturity in this study. Interestingly, the fact that at ripening the protein content did not decrease while amino acids were strongly increased indicates that the latter increase was not due to proteolysis (**Supplemental Figure S3**). In conclusion, when comparing the metabolic shifts that occur throughout the different developmental stages of the melon fruit, characteristic changes in patterns of metabolite

[2]http://primer3.ut.ee/

[3]http://www.r-project.org/

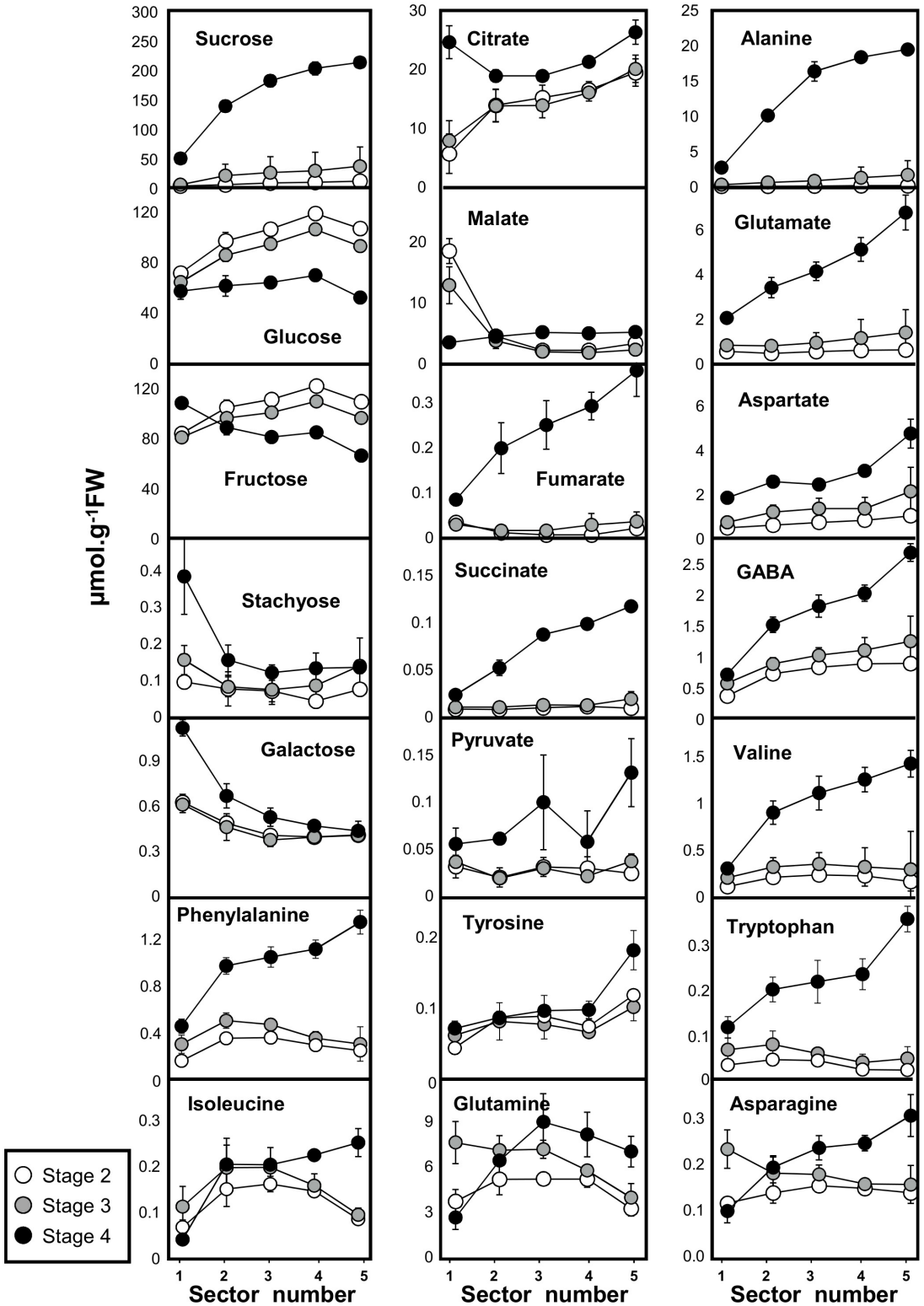

FIGURE 2 | Absolute concentrations in 18 primary metabolites measured by quantitative ^{1}H NMR spectroscopy (16 metabolites) and GC-EI-TOF/MS (pyruvate and succinate) in developing melon (*Cucumis melo* L. var Cantalupensis group Charentais cv. Escrito) fruit harvested at three developmental stages. Sector 1, 2, 3, 4, and 5 correspond to five concentric mesocarp rings taken from the periphery (outer epicarp + green mesocarp, named sector 1) to the fruit centre (inner mescocarp, named sector 5). Concentrations are given in μmol.g^{-1}FW. The results are the means of 9 measurements (3 biological replicates × 3 technical replicates), bars represent standard error (n = 3). The data are available in **Supplemental Table S1**.

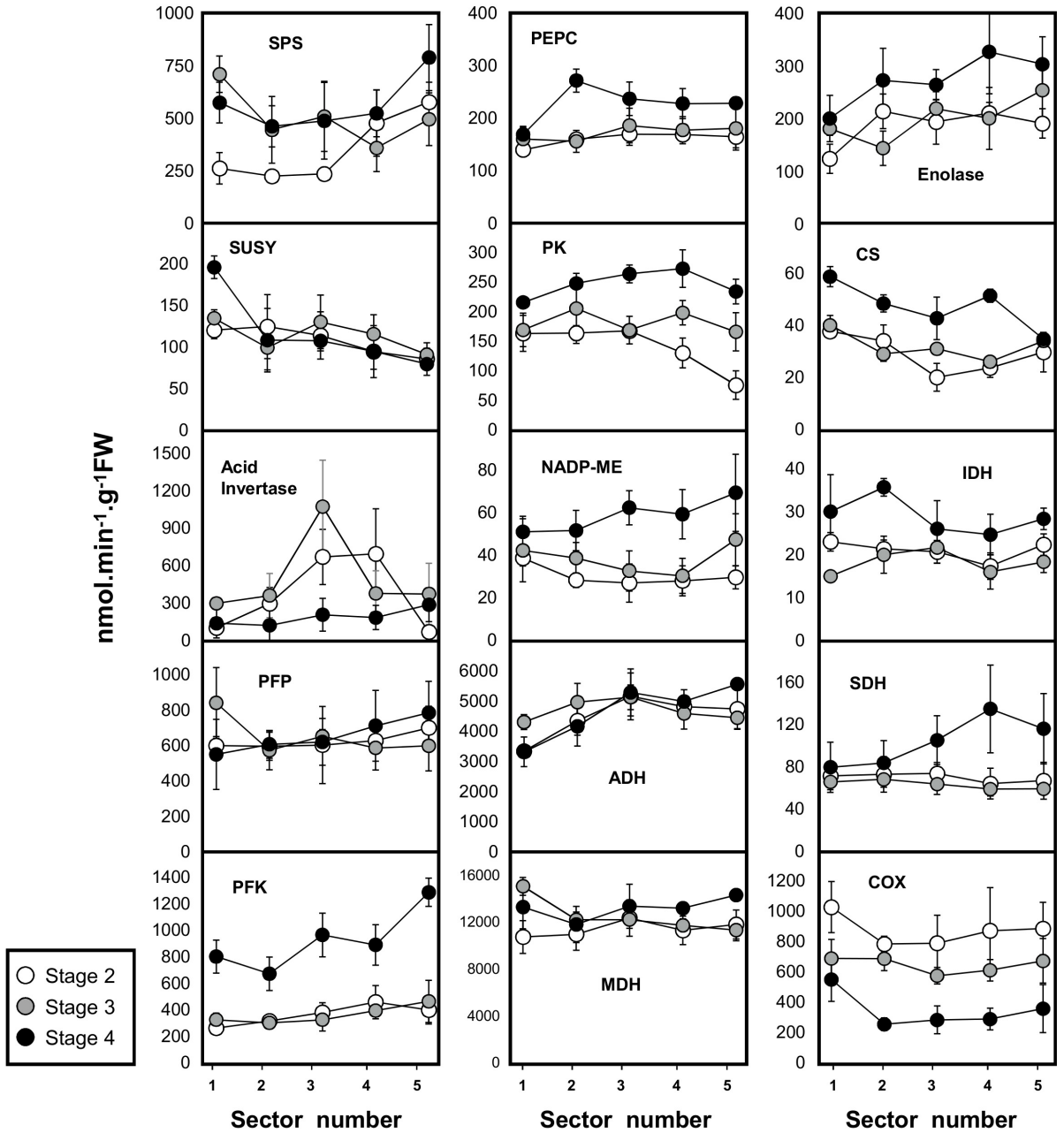

FIGURE 3 | Activities of 15 enzymes from central metabolism during the development of melon (*Cucumis melo* L. var Cantalupensis group Charentais cv. Escrito) fruit harvested at 3 developmental stages. Sector 1, 2, 3, 4, and 5 correspond to five concentric mesocarp rings taken from the periphery (outer epicarp + green mesocarp, named sector 1) to the fruit center (inner mescocarp, named sector 5). Three enzymes involved in sugar metabolism [sucrose synthase (SUSY), acid invertase, sucrose phosphate synthase (SPS)], enolase, 4 glycolytic enzymes [ATP-dependent phosphofructokinase (PFK), pyrophosphate dependent phosphofructokinase (PFP), pyruvate kinase (PK)], 4 enzymes of the tricarboxylic acid cycle [NAD-dependent malate dehydrogenase (MDH), isocitrate dehydrogenase (IDH), citrate synthase (CS), succinate dehydrogenase (SDH)], 2 anaplerotic enzymes [phosphoenolpyruvate carboxylase (PEPC) and NADP malic enzyme (NADP-ME)], 1 enzyme of the respiratory chain [cytochrome c oxidase (COX)] and 1 enzyme involved in fermentation [alcohol dehydrogenase (ADH)]. Enzyme activities are expressed as nmol.g^{-1}FW.min^{-1}. The results are the means of 3 × 3 measurements (3 biological replicates × 3 technical replicates), bars represent standard error (n = 3). The data are available in **Supplemental Table S1**.

accumulation were revealed to be common between amino acids, organic acids and Suc. The gradients observed at different time points and from the periphery to the center of the fruit for amino acids (Ala, Val, Glu, GABA, Asp, Asn, Ile, Phe, Tyr, Trp), organic acids (succinate, fumarate, pyruvate, and citrate) and Suc indicates that the process of maturation starts from the inner part of the fruit. We next therefore investigated whether these metabolic changes were

associated with changes in the activities of enzymes involved in central metabolism.

Most Enzyme Capacities Show Marked Spatial and/or Developmental Gradients

In order to follow metabolic changes in mesocarp tissue during melon fruit development, we profiled capacities (i.e., maximal measurable catalytic activities) of 15 enzymes from central metabolism (**Figure 3**, see also **Supplemental Table S1**). The developmental pattern of Suc accumulation at fruit maturity (stage 4) and the concomitant decrease in Glc and Fru contents were associated to a reduction in acid invertase activity (600–187 nmol.min^{-1}. g^{-1} FW, average of the whole mesocarp at stages 2 and 4). The clear pattern observed for acid invertase was not consistently observed for the two other enzymes involved in Suc metabolism, i.e., SPS and SuSy. A moderate increase in SPS at fruit maturity (stage 4) compared to developing fruit (stage 2) (356–568 nmol.min^{-1}. g^{-1} FW, average of the whole mesocarp at stages 2 and 4) was observed while for SuSy there was a small gradient between the outer and inner mesocarp (sectors 1–5) at all developmental stages (196–80 nmol.min^{-1}. g^{-1} FW, stage 4) (**Figure 3**).

We next explored variations in the capacities of glycolytic enzymes such as ATP-dependent phosphofructokinase (PFK), PPi-dependent phosphofructokinase (PFP), enolase and pyruvate kinase (PK). These four glycolytic enzymes exhibited comparable profiles throughout fruit development. Their activities remained low during stages 2 and 3 while their highest activities were observed at fruit maturity (stage 4). For the four glycolytic enzymes (PFK, PFP, enolase, PK), a net gradient could be observed between sector 1, which corresponds to the green mesocarp below the epicarp, and sectors 2–5, which correspond to the orange mesocarp at full maturity.

Next, the activities of TCA-cycle enzymes, i.e., citrate synthase (CS), NAD-isocitrate dehydrogenase (IDH), SDH and NAD-malate dehydrogenase (MDH), as well as two further enzymes involved in the metabolism of organic acids, i.e., phospho*enol*pyruvate carboxylase (PEPC) and NADP-malic enzyme (ME), were investigated (**Figure 3**). These six activities had comparable profiles during the development of the melon fruit, and peaked at maturity (stage 4). No strong gradient could be observed for these enzymes involved in TCA and organic acid metabolism between the outer and inner mesocarp (except for CS). Conversely, the COX activity of the respiratory chain was relatively high in the mesocarp during stage 1 (871 nmol.min^{-1}. g^{-1} FW average for the whole mesocarp) and, regardless of the location within the tissue, decreased throughout development (down to 346 nmol.min^{-1}. g^{-1} FW average for the whole mesocarp at maturity). A gradient of the COX capacity was also observed between sector 1 corresponding to the green mesocarp, and the orange sectors (from 549 to 259 nmol.min^{-1}.g^{-1} FW at stage 4) (**Figure 3**). Considering that fermentation is particularly important in fruit, ADH was also investigated. ADH activity was high at all three developmental stages and surprisingly high in the external layer of the mesocarp where it reached 3,320 nmol.min^{-1}.g^{-1} FW at stage 2. At maturity, ADH showed the same gradient pattern as the activities of the glycolytic enzymes (PFP, PFK, Enolase, and PK; **Figure 3**).

To summarize, among the 15 tested enzyme activities expressed on a FW basis, only the COX activity of the respiratory chain and acid invertase activities showed a clear decrease at maturity while the other enzymes were stable or tended to slightly increase. The intriguing results obtained with enzymes involved in fermentation (high ADH activity at the periphery and before ripening) and respiration (strong decrease of the COX activity at maturity) prompted us to investigate O_2 availability, as lowering oxygen within the mesocarp might lead to hypoxia and could influence the energy status, which can affect primary metabolism.

Hypoxia Is Gradually Established During the Development of the Melon Fruit Although There Is No Strong Oxygen Gradient Between the Outer- and the Inner Mesocarp

Fine glass microsensors (tip diameter 140 μm) were used to measure O_2 concentrations at three to five different depths in the mesocarp (from 7.5 to 32.5 mm) from three different equatorial positions of fruits harvested across the developmental stages 1–4. The microsensor was introduced into the mesocarp on the equator axis and was driven toward the center of the fruit (**Figure 4A**). Regardless of the developmental status, the O_2 level immediately declined just below the external layer of the mesocarp, from 21 kPa (atmospheric O_2 level) to 16.3 kPa at stage 1 or even to 10.5 kPa at stage 4 (**Figure 4A**). Then, within fruits harvested at stage 1 (developing fruits with a diameter of 80–90 mm), O_2 decreased slightly from 16.3 kPa in the outer layer to 15.5 kPa at 17.5 mm depth. At this developmental stage, all investigated fruits showed similar O_2 profiles. In developing fruits with a diameter of 100–110 mm that are characterized by the absence of the suberized net on the skin (stage 2), the O_2 concentration seemed to be stable regardless of the position on the fruit where it was recorded, but there was a relatively large variability between fruits. Indeed, some fruits at stage 2 showed comparable O_2 concentrations to fruits at stage 1 (around 16.3 kPa), while others showed lower O_2 concentrations (down to 15.5 kPa). These results suggest that fruits selected on the basis of their diameter for stage 2 can in fact be at different developmental stages. The lowest O_2 levels were always detected in early ripening fruits (stage 3), i.e., in fruits with diameter of 130–135 mm (down to 9 kPa). In mature fruit (stage 4), the O_2 concentration was very stable across all tissue sections and types (9.9 kPa). The results show that in the mesocarp O_2 concentrations decrease throughout fruit development and that the O_2 concentration was consistent throughout the whole mesocarp regardless of tissue depth. The relationship between mean O_2 tensions measured in melon fruits harvested at different developmental stages is given in **Figure 4B**. A steady decrease in O_2 was found during the development of melon fruit from stages 1 to 3 and the O_2 tensions remained very stable at around 9.9 ± 0.4 kPa in the whole mesocarp without there being an apparent O_2 gradient in the tissue.

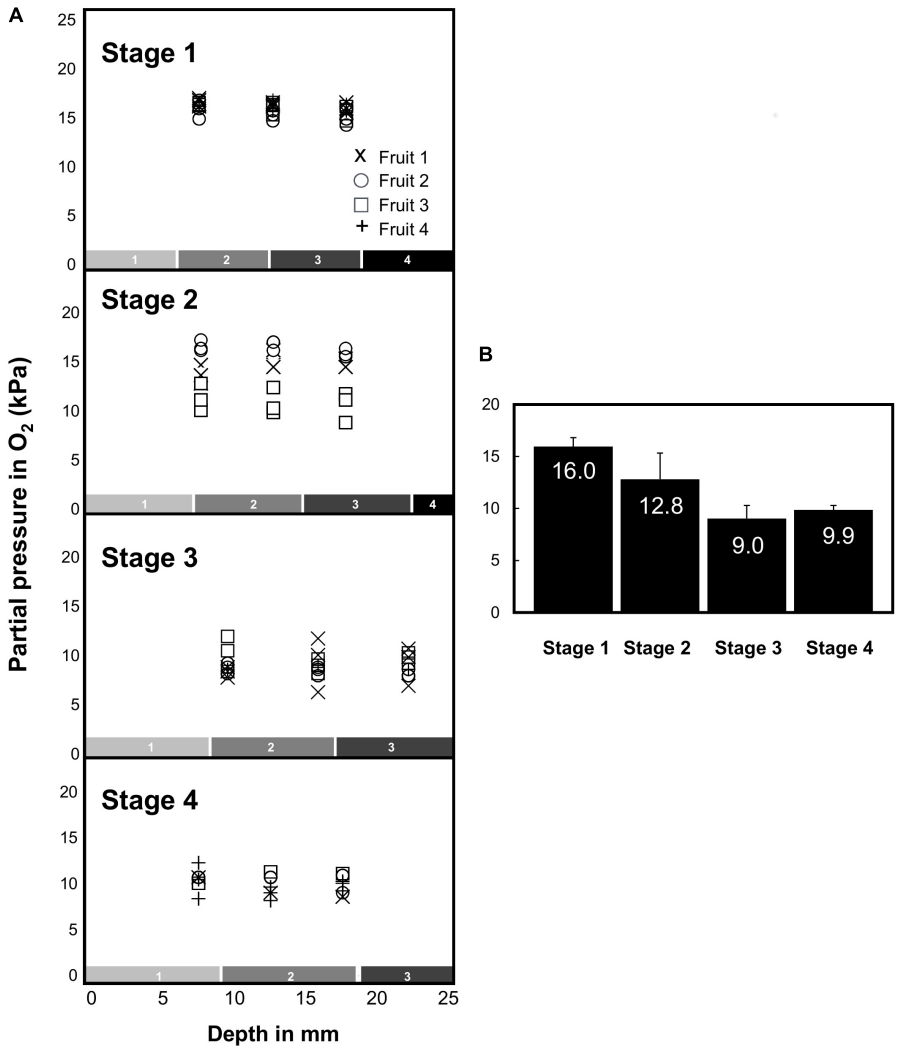

FIGURE 4 | Oxygen tension (expressed in kPa) measured in the mesocarp of 16 melon (*Cucumis melo* L. var Cantalupensis group Charentais cv. Escrito) fruits harvested at stages 1, 2, 3, and 4 with an oxygen-sensitive optical glass-sensor connected to a fiber optic oxygen meter (MicroX TX3 PreSens) based on dynamic fluorescence quenching. **(A)** O_2 tension measured at 3 depths (7.5, 12.5, and 17.5 mm) in the mesocarp and at three different equatorial positions. In mature fruits (stage 4), O_2 tension was measured deeper in the mesocarp (22.5, 27.5, and 32.5 mm). The numbered boxes (gray to black, 1–4) indicate the evolution of the size of the harvested concentric mesocarp ring at stages 1–4. **(B)** Mean O_2 tensions measured in melon fruits harvested at developmental stages 1–4.

Given the intriguing absence of marked gradients in the oxygen concentrations of the mesocarp, it was logical to develop a simple model to predict and analyze the oxygen demand, diffusion, and concentration across the melon flesh.

Oxygen Demand Meets Oxygen Diffusion

Firstly, oxygen demand was calculated from estimates of the rates of biomass production at different depths within the mesocarp (see Materials and Methods). This was first performed by expressing biomass as a function of time for each of the five layers analyzed above (**Supplemental Figure S1**). Fitted polynomials were then integrated to obtain the rates of biomass production and respiration was finally estimated by using a fruit construction cost (process-based) model previously applied to other fleshy fruits, such as tomato, kiwi, peach and grape berry (Liu et al., 2007; Dai et al., 2010, and references therein). Respiratory activity was calculated using either a low or a high estimate of the maintenance-linked respiration (**Supplemental Figure S2**). Next, the oxygen concentration was modeled assuming that a steady state O_2 concentration at any position within the mesocarp is reached when O_2 delivery (diffusion) equals O_2 consumption (respiration). The complete mathematical formulation of this problem has already been described by McElwain (1978) for spherical biological objects. Briefly, the melon was modeled as a homogeneous sphere (i.e., without gas phase in the intercellular space) whose radius varied from stage to stage. Moreover, no O_2 diffusion constraint was supposed to occur outside the melon. In contrast, a constrained diffusion of O_2 across the skin (i.e., h coefficient) and within the mesocarp (i.e., D coefficient) was considered.

Finally, the O_2 gradient was assumed to vanish at the inner limit of the mesocarp, at half of the melon radius. Even though the measured O_2 concentrations within the mesocarp largely exceeded the half saturation constant of the COX, the later parameter was taken into account in our calculations, as in Armstrong and Beckett (2011).

Figure 5 represents the calculated and measured O_2 tensions as a function of the position within the mesocarp and of the developmental stage. Several general trends can be drawn from the simulations. Firstly, the O_2 gradient profile depends on the presence (unbroken line) or not (dashed line) of a gradient of respiratory activity within the tissue. Indeed, parameterizing the growth- and maintenance-dependent O_2 consuming activity gradient with the COX enzymatic activity makes the O_2 gradient flatter regardless of the melon stage. Secondly, the O_2 concentration within the tissue depends on the external O_2 availability, i.e., on the occurrence of diffusion constraints at the melon surface with (blue line) and without (red line) the permeability barrier on the surface of the melon). Indeed, setting a high *h*-value just makes the O_2 concentrations higher within the tissue, the shape of the gradient being unchanged (**Figure 5**).

For each stage, the numerical solutions were compared with the corresponding analytical results (open circles in **Figure 5**). Good agreement between simulations and measurements were obtained when considering both a decrease in the O_2 consumption rate from the surface to the center of the melon and a diffusion constraint at the surface of the melon. A least-square fit of the measured O_2 concentrations gave the highest *h*-values in the earlier stages ($3.7\ 10^{-5}$ and $1.4\ 10^{-5}$ $cm.s^{-1}$ for melons harvested at stages 1 and 2) whereas this permeability coefficient value drastically decreased during later stages, to reach $0.23\ 10^{-5}$ $cm.s^{-1}$ at stage 4 (**Figure 5**). The latter analysis was performed using a high estimate of the maintenance-linked respiration. It should be stressed that similar trends were observed with a low estimate (**Supplemental Figure S4**).

Even though respiratory activity is probably under the control of the major oxidase (i.e., COX), the modeling approach was repeated using the K_m value of alternative oxidase (AOX), which is one order of magnitude higher (0.134 vs. 0.0108 kPa, Armstrong and Beckett, 2011). It is worth mentioning that the O_2 gradient profiles obtained using these values were very similar (**Supplemental Figure S5**). This tends to demonstrate that the affinity of the terminal oxidase of the respiratory chain does not greatly influence the balance between oxygen demand and diffusion throughout melon development (see also Armstrong and Beckett, 2011).

Overall, our modeling approach tends to demonstrate that the melon skin exerts increasing O_2 diffusion constraints during fruit development which, in turn, may favor the establishment of hypoxia within the mesocarp tissue (see **Supplemental Figure S4**). However, the O_2 consumption of this tissue undergoes a spatiotemporal decrease due to a concomitant decrease in the growth rate and the respiratory chain capacity. Therefore, melon development is characterized by a concomitant decrease in both the O_2 demand and

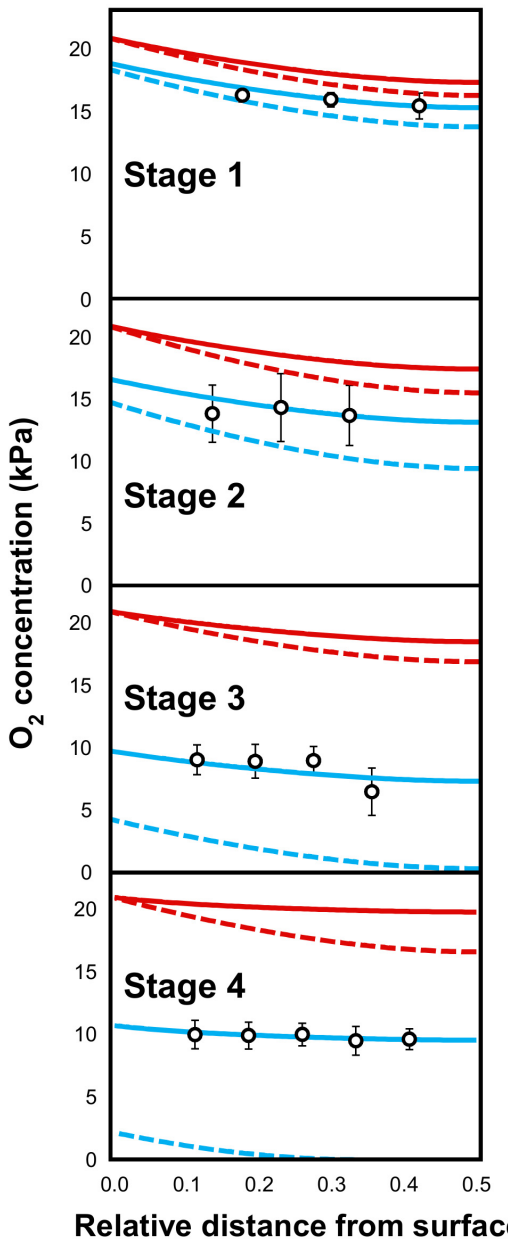

FIGURE 5 | Comparison of measured (open circles) and calculated (red and blue unbroken or dashed lines) O_2 tensions in the mesocarp of melon (*Cucumis melo* L. var Cantalupensis group Charentais cv. Escrito) fruit harvested at stages 1, 2, 3, and 4. O_2 concentration was modeled assuming that a steady state O_2 concentration is reached at any position within the mesocarp when O_2 delivery by diffusion) equals O_2 consumption by respiration. At each stage, a depth-dependent function of the respiratory activity was defined (see **Supplemental Figure S2A**) and the *h*-value (i.e., the permeability coefficient of the melon skin) was optimized to fit the measured O_2 concentrations. Unbroken or dashed lines represent the O_2 gradient profile when a gradient of respiratory activity within the tissue is present or not, respectively. Blue and red lines represent the O_2 concentration within the tissue when a permeability barrier on the surface of the melon occurs (*h*-value is equal to 3.7×10^{-5}, 1.4×10^{-5}, 0.31×10^{-5}, and 0.23×10^{-5} $cm.s^{-1}$ at stages 1, 2, 3, and 4, respectively) or not ($h = 10^{-3}$ $cm.s^{-1}$), respectively. Oxygen concentration is expressed in kPa. A relative distance of 0 corresponds to the melon surface and 0.5, to the inner limit of the mesocarp.

availability, thus ending with O_2 partial pressure values above 40% regardless of the developmental stage and the section of the mesocarp.

Integration of Metabolite Profiles, Enzyme Activities, and O_2 Variables Reveals That the Cytochrome c Oxidase Capacity Is Tuned to Oxygen Availability

Principal component analysis (PCA) was used to integrate metabolite and enzyme data with O_2 demand and concentrations (**Figure 6**). The data for oxygen concentration obtained with the fine glass microsensors did not correspond to the samples used for biochemical analysis and could therefore not be used directly to perform the PCA. Thus, the model described above was used instead, in order to obtain estimates of the oxygen concentration in the different sectors of the mesocarp and at the different developmental stages within which metabolites and enzymes had been measured. Finally, both O_2 demand and O_2 concentration estimates were included within the variables. The PCA was performed with averaged data of estimated oxygen-demand and -concentration, 18 metabolites measured by quantitative ^{1}H NMR spectroscopy and GC-EI-TOF/MS, and 15 enzyme capacities from central metabolism in the five radial sections of the mesocarp expressed on a FW basis (**Supplemental Figure S6**) and on a protein basis (**Figure 6**). The latter gave the best separation of both samples and variables but the general trends were the same for both expression bases. The score plots (**Figures 6A,B**) indicate that the first principal component (PC1), which explains 40% of the total variance, separates the developmental stages whereas PC2, which explains 32% of the total variance, separates the sectors. The scores plots also indicate that the deeper the sector, the larger the amplitude of metabolic change over time. The corresponding loadings plot (**Figure 6C**) highlights four groups of variables, which were clearly associated to growth, ripening, the outer sector 1 (green outer mesocarp) and the inner sectors 2–5. The latter two groups of variables only responded weakly to development (low loadings along PC1). However, in the green outer mesocarp, galactose was closely associated with growth, suggesting that a decrease in carbon demand would lead to a small imbalance between the import and degradation of stachyose. The variable group attributed to growth was also associated with O_2 demand and O_2 concentration (**Figure 6C**). Strikingly, the latter two variables were well correlated with each other ($p = 2.7 \times 10^{-5}$) and with the capacities of the COX ($p = 1.5 \times 10^{-3}$ and 1.6×10^{-6}, respectively) and to a lesser extent SuSy ($p = 3.0 \times 10^{-2}$ and 1.2×10^{-2}, respectively). PFP was also significantly correlated to O_2 concentration ($p = 8.0 \times 10^{-4}$). Glc and Fru, which were highly correlated with each other ($p = 1.6 \times 10^{-12}$), were also positively correlated (p-values ranging from 2.0×10^{-2} to 2.1×10^{-6}) with the previous variables, whereas they were negatively correlated with Suc (p-values ranging from 5.9×10^{-3} to 1.4×10^{-4}). Furthermore, Suc was strongly correlated with pyruvate, Ala, Glu, succinate and fumarate ($p < 3.0 \times 10^{-4}$). ME was also correlated to this group of metabolites. In contrast and as already seen above, changes in ADH were moderately associated to growth, and not to ripening, which implies that the rise in ADH was early during fruit development and not a response to the climacteric crisis.

Tuning of Cytochrome c Oxidase Capacity to Oxygen Availability Is Not Under Transcriptional Control

Because of the strong correlation found between COX capacity on the one hand and O_2 concentration or O_2 demand on the other hand, the expression of genes coding for COX subunits was studied to check whether there is a transcriptional regulation in COX capacity in response to O_2. Given the supramolecular organization of COX, subunits were selected according to their origin (nucleus vs. mitochondrial DNA encoded), their known function (catalysis vs. assembly) and their gene expression change – sometime in opposite directions – in response to oxygen availability (Mansilla et al., 2018). Finally, expression of COX1, COX5b, COX5c, COX6, COX11, and COX15 genes was studied by measuring the concentrations of the corresponding transcripts (**Supplemental Figure S7**). When transcripts were expressed on a protein basis, no significant correlations were found with COX capacity, O_2 concentration or O_2 demand. When transcripts were expressed on a FW basis, negative correlations were found between COX capacity and cox1 ($R^2 = 0.66$, $p = 2.5 \times 10^{-4}$) as well as cox15 ($R^2 = 0.35$, $p = 2 \times 10^{-2}$). O_2 and O_2-demand were also weakly and negatively correlated to cox1 ($R^2 = 0.34$, $p = 0.02$, and $R^2 = 0.42$, $p = 0.009$, respectively). Thus, the link found between COX capacity and O_2 could not be attributed to an adjustment of the expression of these encoding genes.

DISCUSSION

Metabolite Gradients Observed in Melon Fruit Reflect Metabolic Adjustments

The present study confirms that raffinose and stachyose, which are translocated via the phloem in the range of hundreds of mM (Haritatos et al., 1996; Knop et al., 2001), do not accumulate in the fruit flesh, thus indicating a rapid metabolism of these sugars within the fruit. The fact that stachyose and its degradation product galactose sharply decreased from the periphery to the inner mesocarp suggests that carbon import into the mesocarp is mostly centripetal. During fruit growth, glucose, fructose and to a lesser extent citrate were the most abundant metabolites found in the mesocarp. Contrary to stachyose and galactose, these metabolites were increasingly abundant toward the inner part of the mesocarp. This gradient may reflect a spatial difference in sugar metabolism that is perhaps linked to decreasing growth rate and thus decreasing carbon demand when going deeper into the mesocarp.

At ripening, the strong accumulation of a range of metabolites, i.e., sucrose, pyruvate, fumarate, succinate, alanine, glutamate, aspartate, asparagine, valine, and GABA (see also Moing et al.,

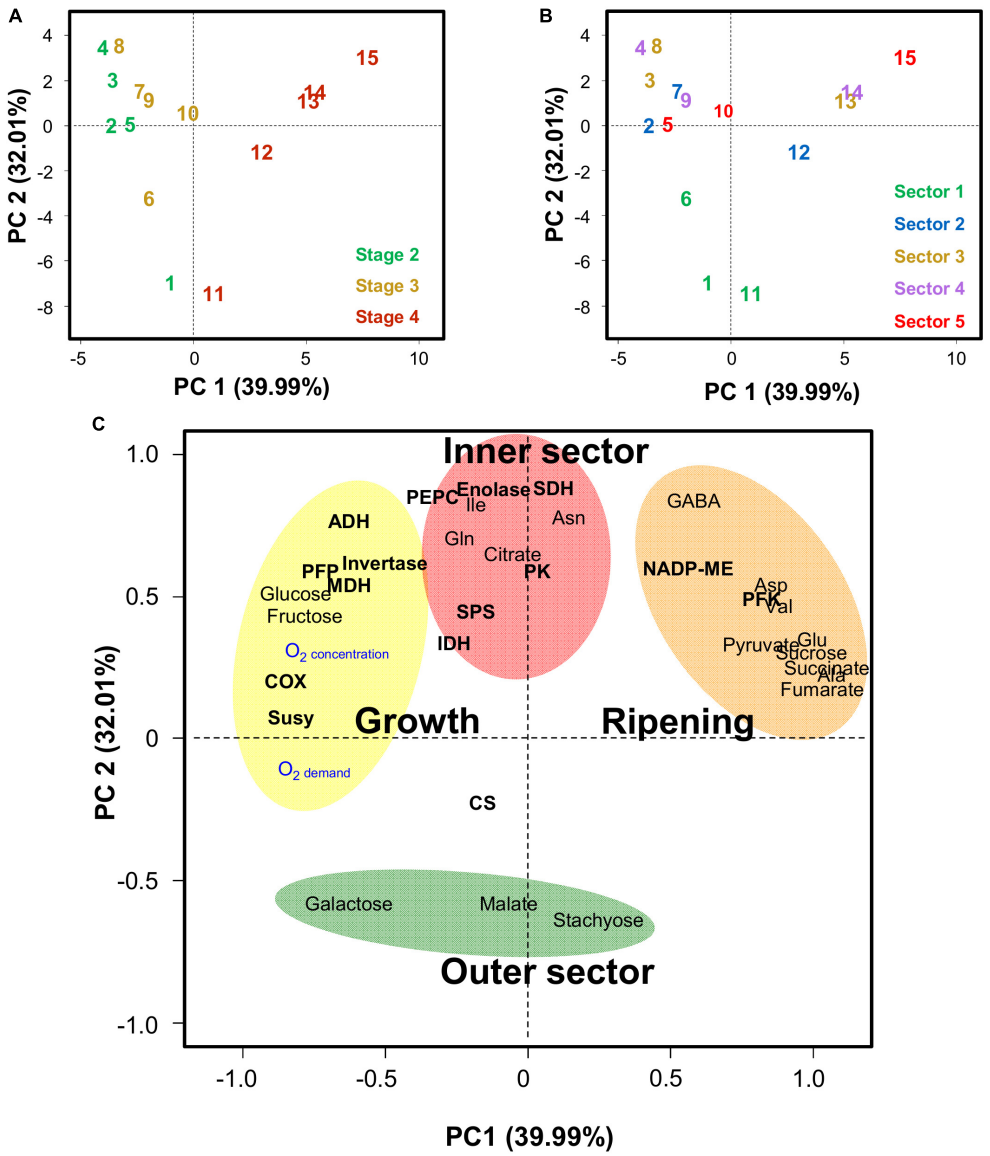

FIGURE 6 | Principal component analysis (PCA) of estimated oxygen-demand and -concentration, 18 metabolites measured by quantitative ^{1}H NMR spectroscopy and GC-EI-TOF/MS, and 15 enzyme capacities from central metabolism in five radial sections of the mesocarp (sector 1, to epicarp + green mesocarp; 5 inner orange mesocarp, see **Figure 1**) of melon (*Cucumis melo* L. var Cantalupensis group Charentais cv. Escrito) fruit at three stages of development, stages 1, 2, and 3. PCA was performed with averaged data expressed on a protein basis and on a FW basis (**Supplemental Figure S6**). **(A)** PCA scores plot of the first two principal components (PC1 and PC2) showing the distribution of the samples at three stages of development. **(B)** Same PCA scores plot of the first two principal components (PC1 and PC2) showing the distribution of the samples from the 5 radial sections of the mesocarp. **(C)** PCA loadings plot showing three different areas. Abbreviations for enzymes are given in the legend of **Figure 3**.

2011), was probably enabled by the arrest of growth that occurred at around growth stage 3. Indeed, assuming that the import and processing of carbon and nitrogen would continue, a decrease in carbon demand would likely result in the accumulation of sugars and organic acids, and a decrease in protein synthesis resulting in the accumulation of amino acids. This accumulation also coincided with a relatively strong drop in the oxygen concentration (on average, from >60% to <50% of the atmospheric concentration), which was probably linked to a drop in the O_2-permeability of the skin (**Figure 5**). Certainly, with the exception of fumarate, these metabolites, which are also precursors of a range of volatiles (Manriquez et al., 2006), are often accumulated in plant tissues under hypoxia (Menegus et al., 1989; Edwards et al., 1998; Roessner et al., 2001; Miyashita et al., 2007; Narsai et al., 2011). Among the enzymes studied here, only PFK and ME continued to accumulate during ripening (**Figures 3**, **6**). Interestingly, the activation of ME under hypoxia has been shown to lead to the accumulation of pyruvate and Ala (Edwards et al., 1998). Besides, the metabolites that accumulated

during ripening, were first seen to accumulate in the inner part of the fruit while oxygen gradients became flatter (they were more marked during growth stages 1–2), indicating that a more marked hypoxia was not the cause of their more pronounced accumulation. The fact that the capacities of most enzymes, in particular ADH and enzymes involved in glycolysis, were already higher in the inner part of the melon at the early growth stages could have potentiated such an accumulation, for example by favoring higher fluxes. Such "priming" phenomenon evokes the increased capacities of a range of enzymes involved in carbon metabolism (including PFP, PFK, Enolase, PK, and ADH), as observed in maize root tips pre-treated by hypoxia and that have been associated with improved survival under subsequent anoxia (Xia et al., 1995; Bouny and Saglio, 1996).

Sucrose Accumulation Is Linked to Fermentation

The large increase in sucrose relative to glucose and fructose that is typically observed in melon has been attributed to the loss of soluble AI and the maintenance of SPS activity during ripening (Schaffer et al., 1987; Hubbard et al., 1989). However, in the present study AI activity was decreased at ripening but not lost, while SPS was maintained or even slightly decreased (**Figure 3**). This is actually in line with a recent study showing that whilst the mRNA of the only expressed gene encoding soluble invertase detected vanished in ripening melon fruits, invertase activity was still detected (Dai et al., 2011). The significantly negative correlation found between sucrose and SuSy suggests that decreasing SuSy may also be necessary for sucrose accumulation. Indeed, the highest SuSy activity was found in the outer mesocarp where sucrose, like stachyose, is probably unloaded from the phloem. Finally, the fact that sucrose was strongly correlated to a group of metabolites known to accumulate under hypoxia raises the question of a possible additional regulation of sucrose turnover by oxygen availability. In line with this, it has been reported that sucrose degradation is quickly inhibited in slices of potato tubers exposed to mild hypoxia (Geigenberger, 2003). Furthermore, in the roots and hypocotyl of soybean seedlings under hypoxia, sucrose has also been found to be accumulated despite maintained acid and alkaline invertase activities (Nanjo et al., 2010).

Melon Fruit Achieves the Avoidance of Oxygen Gradient Within the Mesocarp

Oxygen gradients linked to oxygen diffusion have been reported for a range of plant systems. For example, potato tubers (Bologa et al., 2003) or soybean developing seeds (Borisjuk and Rolletschek, 2009) show dramatic O_2 gradients when under optimal growth conditions, with the root nodules of legumes even achieving anoxic conditions within their center, an absolute requirement for N-fixation (Ott et al., 2005). Surprisingly, there were no such gradients in the mesocarp of melon fruit, even though hypoxia takes place and despite the fact that melons are relatively fast growing fruits that reach remarkably large sizes. A simple explanation is that the spherical form of the fruit guarantees that the O_2 demand decreases from the outside to the inside, simply because there is considerably less biomass being produced in the inside than at the periphery. The model integrating O_2 diffusion and demand presented here confirms this hypothesis.

Additionally, it is likely that mechanisms avoiding the waste of O_2 taking place across the developmental stages studied here were also modulating the consumption of O_2. Thus, SuSy and PFP, which were associated to the outer mesocarp where O_2-demand was highest, are both considered as energy saving enzymes. The breakdown of Suc into hexose phosphates requires only one PPi when initiated via SuSy and two ATP when initiated via invertase (Geigenberger, 2003). Similarly, the phosphorylation of fructose-6P costs one PPi via PFP and one ATP via PFK, which again saves energy, especially in growing tissues where PPi is produced at high rates (Stitt, 1998). It is also striking that PFK activity increased quite dramatically at ripening, although O_2-availability was decreased. It suggests that ATP-usage was no longer critical and/or that it was required to replace PPi-dependent reactions because PPi production had dropped, both events being consequences of arrested growth. This is in line with a recent study carried out on tomato pericarp which demonstrated that the energy-saving priority of fruit growth vanishes at the end of development thus leading to the onset of the climacteric crisis (Colombie et al., 2017).

Finally, the most remarkable metabolic adjustment to fluctuating O_2 discovered by this study was the tuning of the capacity of COX to O_2-availability. It is worth mentioning that such hypotheses are strongly debated in the literature (Armstrong and Beckett, 2011; Nikoloski and van Dongen, 2011). In plant cells, the local O_2 tension results in a balance between oxygen diffusivity within the tissue and the activity of the oxygen consuming enzymes, especially COX, which is involved in the mitochondrial oxidative phosphorylation pathway. In dense, metabolically active and growing tissues such as seeds, seedlings, tubers and fleshy fruits, the lack of systems for O_2 distribution leads to the limitation of oxygen diffusion, which may lead to a fall in the internal O_2 concentrations (Borisjuk and Rolletschek, 2009). Admittedly, a falling internal O_2 concentration results in a restriction of metabolic activity (Geigenberger, 2003). Within potato tubers (Geigenberger et al., 2000), pea and bean seeds (Rolletschek et al., 2002), it is paralleled by a severe decrease in the ATP/ADP ratio and adenylate energy charge (AEC), indicating that respiration is being inhibited. In melon fruits, despite a drastic decrease in ATP/ADP, from 31 (outer mesocarp) to 6 (inner mesocarp), the AEC is only slightly decreased, from 0.97 in the outer mesocarp to 0.83 in the inner mesocarp (Biais et al., 2009). As reported by Pradet and Raymond (1983), small variations in AEC with high values (between 0.85 and 0.95) imply significant variations in the ATP/ADP and ATP/AMP ratios and may thus conceal quite different regulatory situations for enzymatic ATP-utilizing processes. In a developing melon fruit, relatively high AEC and low ATP/ADP suggest

that ATP-generating pathways (i.e., glycolysis and oxidative phosphorylation) are fitting the energy supply to the demands of the processes involved in growth and maintenance. Changes in both ATP/ADP and AEC have been observed *in vitro* and *in vivo* in potato tubers (Geigenberger et al., 2000) and tomato pericarp (Menu et al., 2004) under conditions of artificially low atmospheric oxygen pressure. Most importantly, the present study indicates that in melon fruit placed under atmospheric oxygen tension the decrease in the ATP/ADP ratio observed from the periphery to the inner mesocarp is not the consequence of an oxygen gradient within the tissue but rather a decrease in the capacity of the respiratory chain (i.e., the COX activity). Importantly, the affinity of COX for O_2 corresponds to O_2 concentrations that are much lower than those reported here, which suggests that regulatory events involving oxygen-sensing (Licausi et al., 2011; Weits et al., 2014) are taking place. The modulation of the capacity of COX therefore appears as a potent metabolic adjustment avoiding hypoxia. COX is usually considered as the rate-controlling step of the oxidative phosphorylation pathway. In various aerobically growing cells, down-regulation of COX activity participates to a fine-tuning of the respiratory capacity to changes in ATP demand, thus leading to energy status homeostasis (Devin et al., 2006). Here, our measurements provide evidence that the modulation of COX capacity (V_{max}), rather than its apparent affinity for O_2 (K_m), can explain, at least in part, the spatiotemporal changes in the O_2 concentration that are observed in bulky growing plant organs such as fleshy fruits. Transcriptional regulation is unlikely to occur in melon fruit since the transcript levels of nuclear- and mitochondria-encoded COX genes, especially COX5b and COX5c which are known to be downregulated by O_2 deprivation in rice (Tsuji et al., 2000) sunflower (Curi et al., 2002) and Arabidopsis thaliana (Mansilla et al., 2018), were not positively correlated to the COX activity nor to the local O_2 concentration. Therefore, mechanisms underlying the down-regulation of COX activity remain to be elucidated. However, it is clear that these changes do not result from a down-modulation of the mitochondria biogenesis *per se* (i.e., mitochondria content) since the evolution patterns of COX did not parallel with those of other mitochondrial enzymes (i.e., SDH, CS, and IDH). However, a modulation of the COX activity by means of post-translational modifications of regulatory subunits (Mansilla et al., 2018) is not to be excluded under our conditions.

Skin as a Key Factor Controlling Hypoxia-Driven Maturation of the Melon Fruit

Oxygen deprivation is usually seen as leading to a serious disruption of plant metabolism, which is essentially an aerobic process (Geigenberger, 2003). As discussed above, melon fruit appears to be capable of maintaining a low-slope gradient of O_2 concentrations throughout the mesocarp and at different developmental stages, especially during ripening where O_2 concentrations were lowest (nearly 9 kPa corresponding to 40% of atmospheric O_2). However, despite these mechanisms, the entire mesocarp became hypoxic quite early during fruit development (at stage 1, the average O_2 concentration was already decreased by 24%). The modeling approach developed in the present study suggests that this was due to changes in skin permeability to O_2. These computations are in line with gas transport measurements performed on pear and apple tissues showing that skin has a 20–50-fold lower O_2 diffusibility than flesh (Ho et al., 2006, 2011). So, why would melon fruit build a skin that provokes hypoxia? Firstly, in many fruit species fermentative metabolic features are essential for the production of aroma volatiles during ripening (Manriquez et al., 2006). Hypoxia and/or products of fermentation such as ethanol and acetaldehyde are also triggers of fruit maturation (Pesis, 2005). Secondly, oxygen- and ethylene sensing mechanisms are known to interact at the molecular level within plants (Bailey-Serres et al., 2012), as well as fruits (Min et al., 2012), and oxygen promotes ripening in climacteric fruits by stimulating the ethylene response via a mechanism that obeys Michaelis–Menten kinetics (Beaudry, 1999). Therefore, decreasing internal O_2 concentrations can also be seen as a way of controlling the rate of ripening.

CONCLUSION

Taken together our results show that the entire mesocarp becomes hypoxic quite early during fruit development and suggest that in developing melon fruits O_2 supply and O_2 consumption are finely tuned by a combination of factors to ensure a timely maturation of the mesocarp. The spherical form of the fruit combined with the metabolic adjustments, especially the tuning of the capacity of COX to O_2 availability that occurs during growth contribute to optimizing the O_2 demand and avoiding the establishment of an O_2 gradient within the flesh. The fact that such "controlled" hypoxia occurs relatively early in the fruit's development would favor the increased activity of a range of enzymes involved in glycolysis and fermentation and that are essential for maturation. In addition the modeling approach developed in the present study suggests that the decrease in the skin permeability to O_2 that coincides with the climacteric peak would moderate ripening while favoring fermentation throughout the mesocarp and almost at the same time, thus ensuring uniform maturation of the melon flesh. Skin permeability for oxygen therefore appears as a particularly interesting trait to investigate, especially in relation to metabolism, in further melon varieties and fruit species, as it could lead to improvements of fruit quality.

The assay for COX developed here is relatively easy to perform, thus providing an opportunity to investigate bulky organs in other species to verify whether COX adjustment to oxygen availability is a generic mechanism. The fact that the assay can also be performed in high throughput could then open a range of reverse and forward genetic approaches to investigate and manipulate hypoxia in plants. It will indeed be particularly

interesting to try to investigate the regulation of respiration in relation to oxygen availability.

DATA AVAILABILITY

The datasets for this manuscript are not publicly available because the data are provided in the **Supplementary Data** of the present manuscript. Requests to access the datasets should be directed to yves.gibon@inra.fr.

AUTHOR CONTRIBUTIONS

KM, BPB, DR, AM, and YG planned the experiments. KM, BPB, BB, MC, JA, CD, MM, RG, CC, and AM performed the experiments. KM, BPB, DR, and YG interpreted the data and wrote the manuscript. All authors have read and approved the manuscript.

FUNDING

This work was supported by EU FP6 META-PHOR (FOOD–CT–2006–036220), ANR MetaboHUB (ANR-11-INBS-0010) and ANR PHENOME (ANR-11-INBS-0012).

ACKNOWLEDGMENTS

We thank S. Bochu and F. Leix-Henry (CEFEL, France) and E. Sclaunich (INVENIO, France) for providing the fruits.

SUPPLEMENTARY MATERIAL

The Supplementary Material for this article can be found online at: https://www.frontiersin.org/articles/10.3389/fpls.2019.00594/full#supplementary-material

REFERENCES

Allwood, J. W., Cheun, W., Xua, Y., Mumm, R., de Vos, R. C. H., Deborde, C., et al. (2014). Metabolomics in melon: a new opportunity for aroma analysis. *Phytochemistry* 99, 61–72. doi: 10.1016/j.phytochem.2013.12.010

Allwood, J. W., Erban, A., de Koning, S., Dunn, W. B., Luedemann, A., Lommen, A., et al. (2009). Inter-laboratory reproducibility of fast gas chromatography–electron impact–time of flight mass spectrometry (GC–EI–TOF/MS) based plant metabolomics. *Metabolomics* 5, 479–496. doi: 10.1007/s11306-009-0169-z

Armstrong, W., and Beckett, P. M. (2011). Experimental and modelling data contradict the idea of respiratory down-regulation in plant tissues at an internal [O2] substantially above the critical oxygen pressure for cytochrome oxidase. *New Phytol.* 190, 431–441. doi: 10.1111/j.1469-8137.2010.03537.x

Bailey-Serres, J., Fukao, T., Gibbs, D. J., Holdsworth, M. J., Lee, S. C., Licausi, F., et al. (2012). Making sense of low oxygen sensing. *Trends Plant Sci.* 17, 129–138. doi: 10.1016/j.tplants.2011.12.004

Beaudry, R. M. (1999). Effect of O2 and CO2 partial pressure on selected phenomena affecting fruit and vegetable quality. *Postharvest Biol. Technol.* 15, 293–303. doi: 10.1016/s0925-5214(98)00092-1

Bernillon, S., Biais, B., Deborde, C., Maucourt, M., Cabasson, C., Gibon, Y., et al. (2013). Metabolomic and elemental profiling of melon fruit quality as affected by genotype and environment. *Metabolomics* 9, 57–77. doi: 10.1007/s11306-012-0429-1

Biais, B., Allwood, J. W., Deborde, C., Xu, Y., Maucourt, M., Beauvoit, B., et al. (2009). 1H-NMR, GC-EI-TOF/MS and data set correlation for fruit metabolomics, application to spatial metabolite analysis in melon. *Anal. Chem.* 81, 2884–2894. doi: 10.1021/ac9001996

Biais, B., Beauvoit, B., Allwood, J. W., Deborde, C., Maucourt, M., Goodacre, R., et al. (2010). Metabolic acclimation to hypoxia revealed by metabolite gradients in melon fruit. *J. Plant Physiol.* 167, 242–245. doi: 10.1016/j.jplph.2009.08.010

Bologa, K. L., Fernie, A. R., Leisse, A., Loureiro, M. E., and Geigenberger, P. (2003). A bypass of sucrose synthase leads to low internal oxygen and impaired metabolic performance in growing potato tubers. *Plant Physiol.* 132, 2058–2072. doi: 10.1104/pp.103.022236

Borisjuk, L., and Rolletschek, H. (2009). The oxygen status of the developing seed. *New Phytol.* 182, 17–30. doi: 10.1111/j.1469-8137.2008.02752.x

Bouny, J. M., and Saglio, P. H. (1996). Glycolytic flux and hexokinase activities in anoxic maize root tips acclimated by hypoxic pretreatment. *Plant Physiol.* 111, 187–194. doi: 10.1104/pp.111.1.187

Bradford, M. M. (1976). A rapid and sensitive method for the quantification of microgram quantities of proteins utilizing the principle of protein-dye binding. *Anal. Biochem.* 72, 248–254. doi: 10.1006/abio.1976.9999

Burell, M. M., Mooney, P. J., Blundy, M., Carter, D., Wilson, F., Green, J., et al. (1994). Genetic manipulation of 6-phosphofructokinase in potato tubers. *Planta* 194, 95–101. doi: 10.1007/BF00201039

Burger, Y., and Schaffer, A. A. (2007). The contribution of sucrose metabolism enzymes to sucrose accumulation in *Cucumis melo*. *J. Am. Soc. Hortic. Sci.* 132, 704–712. doi: 10.21273/jashs.132.5.704

Burger, Y., Shen, S., Petreikov, M., and Schaffer, A. A. (2000). The contribution of sucrose to total sugar content in melons. *Acta Hortic.* 510, 479–485.

Cohen, S., Itkin, M., Yeselson, Y., Tzuri, G., Portnoy, V., Harel-Baja, R., et al. (2014). The PH gene determines fruit acidity and contributes to the evolution of sweet melons. *Nat. Commun.* 5:4026. doi: 10.1038/ncomms5026

Colombie, S., Beauvoit, B., Nazaret, C., Benard, C., Vercambre, G., Le Gall, S., et al. (2017). Respiration climacteric in tomato fruits elucidated by constraint-based modelling. *New Phytol.* 213, 1726–1739. doi: 10.1111/nph.14301

Curi, G. C., Chan, R. L., and Gonzalez, D. H. (2002). Genes encoding cytochrome c oxidase subunit 5c from sunflower (*Helianthus annuus* L.) are regulated by nitrate and oxygen availability. *Plant Sci.* 2002, 897–905. doi: 10.1016/s0168-9452(02)00237-6

Dai, N., Cohen, S., Portnoy, V., Tzuri, G., Harel-Beja, R., Pompan-Lotan, M., et al. (2011). Metabolism of soluble sugars in developing melon fruit: a global transcriptional view of the metabolic transition to sucrose accumulation. *Plant Mol. Biol.* 76, 1–18. doi: 10.1007/s11103-011-9757-1

Dai, Z. W., Vivin, P., Barrieu, F., Ollat, N., and Delrot, S. (2010). Physiological and modelling approaches to understand water and carbon fluxes during grape berry growth and quality development: a review. *Aust. J. Grape Wine Res.* 16, 70–85. doi: 10.1111/j.1755-0238.2009.00071.x

Devin, A., Dejean, L., Beauvoit, B., Chevtzoff, C., Avéret, N., Bunoust, O., et al. (2006). Growth-yield homeostasis in respiring yeast is due to a strict mitochondrial content adjustment. *J. Biol. Chem.* 281, 26779–26784. doi: 10.1074/jbc.m604800200

Edwards, S., Nguyen, B. T., Do, B., and Roberts, J. K. M. (1998). Contribution of malic enzyme, pyruvate kinase, phosphoenolpyruvate carboxylase, and the krebs cycle to respiration and biosynthesis and to intracellular pH regulation during hypoxia in maize root tips observed by nuclear magnetic resonance imaging and gas chromatography mass spectrometry. *Plant Physiol.* 116, 1073–1081. doi: 10.1104/pp.116.3.1073

Fiehn, O. (2003). Metabolic networks of *Cucurbita maxima* phloem. *Phytochemistry* 62, 875–886. doi: 10.1016/s0031-9422(02)00715-x

Geigenberger, P. (2003). Response of plant metabolism to too little oxygen. *Curr. Opin. Plant Biol.* 6, 247–256. doi: 10.1016/s1369-5266(03)00038-4

Geigenberger, P., Fernie, A. R., Gibon, Y., Christ, M., and Stitt, M. (2000). Metabolic activity decreases as an adaptive response to low internal oxygen in growing potato tubers. *Biol. Chem.* 381, 723–740.

Gibon, Y., Blaesing, O. E., Hannemann, J., Carillo, P., Höhne, M., Hendriks, J. H., et al. (2004). A robot-based platform to measure multiple enzyme activities in *Arabidopsis* using a set of cycling assays: comparison of changes of enzyme activities and transcript levels during diurnal cycles and in prolonged darkness. *Plant Cell* 16, 3304–3325. doi: 10.1105/tpc.104.025973

Gibon, Y., Pyl, E. T., Sulpice, R., Lunn, J. E., Höhne, M., Günther, M., et al. (2009). Adjustment of growth, starch turnover, protein content and central metabolism to a decrease of the carbon supply when *Arabidopsis* is grown in very short photoperiods. *Plant Cell Environ.* 32, 859–874. doi: 10.1111/j.1365-3040.2009.01965.x

Gibon, Y., Usadel, B., Blaesing, O. E., Kamlage, B., Hoehne, M., Trethewey, R., et al. (2006). Integration of metabolite with transcript and enzyme activity profiling during diurnal cycles in *Arabidopsis* rosettes. *Genome Biol.* 7:R76.

Haritatos, E., Keller, F., and Turgeon, R. (1996). Raffinose oligosaccharide concentrations measured in individual cell and tissue types in *Cucumis melo* L. leaves implications for phloem loading. *Planta* 198, 614–622. doi: 10.1007/BF00262649

Heuvelink, E. (1995). Dry matter production in a tomato crop: measurements and simulation. *Ann. Bot.* 75, 369–379. doi: 10.1006/anbo.1995.1035

Ho, Q. T., Verboven, P., Verlinden, B. E., Herremans, E., Wevers, M., Carmeliet, J., et al. (2011). A three-dimensional multiscale model for gas exchange in fruit. *Plant Physiol.* 155, 1158–1168. doi: 10.1104/pp.110.169391

Ho, Q. T., Verlinden, B. E., Verboven, P., and Nicolaï, B. M. (2006). Gas diffusion properties at different positions in the pear. *Postharvest Biol. Technol.* 41, 113–120. doi: 10.1016/j.postharvbio.2006.04.002

Hubbard, N. L., Huber, S. C., and Pharr, D. M. (1989). Sucrose phosphate synthase and acid invertase as determinates of sucrose concentration in developing muskmelon (*Cucumis melo*, L.). fruits. *J. Am. Soc. Hortic. Sci.* 91, 1527–1534. doi: 10.1104/pp.91.4.1527

Iwatsubo, T., Nakagawa, H., Ogura, N., Hirabayashi, T., and Sato, T. (1992). Acid invertase of melon fruits: immunochemical detection of acid invertases. *Plant Cell Physiol.* 33, 1127–1133.

Knop, C., Voitsekhovskaja, O., and Lohaux, G. (2001). Sucrose transporters in two members of the *Scrophulariaceae* with different types of transport sugar. *Planta* 213, 80–91. doi: 10.1007/s004250000465

Lê, S., Josse, J., and Husson, F. (2008). FactoMineR: an R package for multivariate analysis. *J. Stat. Softw.* 25, 1–18.

Lester, G. E., Arias, L. S., and Gomez-Lim, M. (2001). Muskmelon fruit soluble acid invertase and sucrose phosphate activity and polypeptide profiles during growth and maturation. *J. Am. Soc. Hortic. Sci.* 126, 33–36. doi: 10.21273/jashs.126.1.33

Licausi, F., Kosmacz, M., Weits, D. A., Giuntoli, B., Giorgi, F. M., Voesenek, L. A. C. J., et al. (2011). Oxygen sensing in plants is mediated by an N-end rule pathway for protein destabilization. *Nature* 479, 419–422. doi: 10.1038/nature10536

Lingle, S. E., and Dunlap, J. R. (1987). Sucrose metabolism in netted muskmelon fruit during development. *Plant Physiol.* 84, 386–389. doi: 10.1104/pp.84.2.386

Liu, H. F., Génard, M., Guichard, S., and Bertin, N. (2007). Model-assisted analysis of tomato fruit growth in relation to carbon and water fluxes. *J. Exp. Bot.* 58, 3567–3580. doi: 10.1093/jxb/erm202

Manriquez, D., El-Sharkawy, I., Flores, F. B., El-Yahyaoui, F., Regad, F., Bouzayen, M., et al. (2006). Two highly divergent alcohol dehydrogenases of melon exhibit fruit ripening-specific expression and distinct biochemical characteristics. *Plant Mol. Biol.* 61, 675–685. doi: 10.1007/s11103-006-0040-9

Mansilla, N., Racca, S., Gras, D. E., Gonzales, D. H., and Welchen, E. (2018). The complexity of mitochondrial complex IV: an update of cytochrome c oxidase biogenesis in plants. *Int. J. Mol. Sci.* 19:662. doi: 10.3390/ijms19030662

McCollum, T. G., Huber, D. J., and Cantliffe, D. J. (1988). Soluble sugar accumulation and activity of related enzymes during muskmelon fruit development. *J. Am. Soc. Hortic. Sci.* 113, 399–403.

McElwain, D. L. (1978). A re-examination of oxygen diffusion in a spherical cell with michaelis-menten oxygen uptake kinetics. *J. Theor. Biol.* 71, 255–263. doi: 10.1016/0022-5193(78)90270-9

Menegus, F., Cattaruzza, L., Chersi, A., and Fronza, G. (1989). Differences in the anaerobic lactate-succinate production and in the changes of cell sap pH for plants with high and low resistance to anoxia. *Plant Physiol.* 90, 29–32. doi: 10.1104/pp.90.1.29

Menu, T., Saglio, P., Granot, D., Dai, N., Raymond, P., and Ricard, B. (2004). High hexokinase activity in tomato fruit perturbs carbon and energy metabolism and reduces fruit and seed size. *Plant Cell Environ.* 27, 89–98. doi: 10.1046/j.0016-8025.2003.01128.x

Min, T., Yin, X. R., Shi, Y. N., Luo, Z. R., Yao, Y. C., Grierson, D., et al. (2012). Ethylene-responsive transcription factors interact with promoters of ADH and PDC involved in persimmon (*Diospyros kaki*) fruit de-astringency. *J. Exp. Bot.* 63, 6393–6405. doi: 10.1093/jxb/ers296

Mitchell, D. E., Gadus, M. V., and Madore, M. A. (1992). Patterns of assimilate production and translocation in muskmelon (*Cucumis melo* L.): I. diurnal patterns. *Plant Physiol.* 99, 959–965. doi: 10.1104/pp.99.3.959

Miyashita, Y., Dolferus, R., Ismond, K. P., and Good, A. G. (2007). Alanine aminotransferase catalyses the breakdown of alanine after hypoxia in *Arabidopsis thaliana*. *Plant J.* 49, 1108–1121. doi: 10.1111/j.1365-313x.2006.03023.x

Moing, A., Aharoni, A., Biais, B., Rogachev, I., Meir, S., Brodsky, L., et al. (2011). Extensive metabolic cross-talk in melon fruit revealed by spatial and developmental combinatorial metabolomics. *New Phytol.* 190, 683–696. doi: 10.1111/j.1469-8137.2010.03626.x

Mounet, F., Lemaire-Chamley, M., Maucourt, M., Cabasson, C., Giraudel, J. L., Deborde, C., et al. (2007). Quantitative metabolic profiles of tomato flesh and seeds during fruit development: complementary analysis with ANN and PCA. *Metabolomics* 3, 273–288. doi: 10.1007/s11306-007-0059-1

Nanjo, Y., Skultety, L., Ashraf, Y., and Komatsu, S. (2010). Comparative proteomic analysis of early-stage soybean seedlings responses to flooding by using gel and gel-free techniques. *J. Proteome Res.* 9, 3989–4002. doi: 10.1021/pr100179f

Narsai, R., Rocha, M., Geigenberger, P., Whelan, J., and van Dongen, J. T. (2011). Comparative analysis between plant species of transcriptional and metabolic responses to hypoxia. *New Phytol.* 190, 472–487. doi: 10.1111/j.1469-8137.2010.03589.x

Nikoloski, Z., and van Dongen, J. T. (2011). Modelling alternatives for interpreting the change in oxygen-consumption rates during hypoxic conditions. *New Phytol.* 190, 273–276. doi: 10.1111/j.1469-8137.2011.03674.x

Ott, T., van Dongen, J. T., Gunther, C., Krusell, L., Desbrosses, G., Vigeolas, H., et al. (2005). Symbiotic leghemoglobins are crucial for nitrogen fixation in legume root nodules but not for general plant growth and development. *Curr. Biol.* 15, 531–535. doi: 10.1016/j.cub.2005.01.042

Pesis, E. (2005). The role of the anaerobic metabolites, acetaldehyde and ethanol, in fruit ripening, enhancement of fruit quality and fruit deterioration. *Postharvest Biol. Technol.* 37, 1–19. doi: 10.1016/j.postharvbio.2005.03.001

Piques, M., Schulze, W. X., Hohne, M., Usadel, B., Gibon, Y., Rohwer, J., et al. (2009). Ribosome and transcript copy numbers, polysome occupancy and enzyme dynamics in *Arabidopsis*. *Mol. Syst. Biol.* 5:314. doi: 10.1038/msb.2009.68

Pradet, A., and Raymond, P. (1983). Adenine nucleotide ratios and adenylate energy charge in energy metabolism. *Ann. Rev. Plant Physiol.* 34, 199–224. doi: 10.1146/annurev.pp.34.060183.001215

Pyl, E.-T., Piques, M., Ivakov, A., Schulze, W., Ishihara, H., Stitt, M., et al. (2012). Metabolism and growth in *Arabidopsis* depend on the daytime temperature but are temperature-compensated against cool nights. *Plant Cell* 24, 2443–2469. doi: 10.1105/tpc.112.097188

Roessner, U., Luedemann, A., Brust, D., Fiehn, O., Linke, T., Willmitzer, L., et al. (2001). Metabolic profiling allows comprehensive phenotyping of genetically or environmentally modified plant systems. *Plant Cell* 13, 11–29. doi: 10.1105/tpc.13.1.11

Rolletschek, H., Borisjuk, L., Koschorreck, M., Wobus, U., and Weber, H. (2002). Legume embryos develop in a hypoxic environment. *J. Exp. Bot.* 53, 1099–1107. doi: 10.1093/jexbot/53.371.1099

Rustin, P., Chretien, D., Bourgeron, T., Gérard, B., Rotig, A., Saudubray, J. M., et al. (1994). Biochemical and molecular investigations in respiratory chain deficiencies. *Clin. Chim. Acta* 228, 35–51. doi: 10.1016/0009-8981(94)90055-8

Schaffer, A. A., Aloni, B., and Fogelman, E. (1987). Sucrose metabolism and accumulation in developing fruit of *Cucumis*. *Phytochemistry* 26, 1883–1887. doi: 10.1016/s0031-9422(00)81721-5

Steinhauser, M. C., Steinhauser, D., Koehl, K., Carrari, F., Gibon, Y., Fernie, A. R., et al. (2010). Enzyme activity profiles during fruit development in tomato cultivars and *Solanum pennellii*. *Plant Physiol.* 153, 80–98. doi: 10.1104/pp.110.154336

Stitt, M. (1998). Pyrophosphate as an energy donor in the cytosol of plant cells: an enigmatic alternative to ATP. *Bot. Acta* 111, 167–175. doi: 10.1111/j.1438-8677.1998.tb00692.x

Studart-Guimaräes, C., Gibon, Y., Frankel, N., Wood, C., Zanor, M., Fernie, A., et al. (2005). Identification and characterisation of the α and β subunits of succinyl CoA ligase of tomato. *Plant Mol. Biol.* 59, 781–791. doi: 10.1007/s11103-005-1004-1

Tang, M., Zhang, B.-C., Xie, J.-J., Bie, Z.-L., Wu, M.-Z., Yi, H.-P., et al. (2012). Sucrose and citric acid accumulations in melon genotypes with different sugar and acid contents. *J. Food Agric. Environ.* 10, 225–231.

Tsuji, H., Nakazono, M., Saisho, D., Tsutsumi, N., and Hirai, A. (2000). Transcript levels of the nuclear-encoded respiratory genes in rice decrease by oxygen deprivation: evidence for involvement of calcium in expression of the alternative oxidase 1a gene. *FEBS Lett.* 471, 201–204. doi: 10.1016/s0014-5793(00)01411-3

Vinogradov, A. D., Gavrikov, V. G., and Gavrikova, E. V. (1980). Studies on the succinate dehydrogenating system. ii. reconstitution of succinate-ubiquinone reductase from the soluble components. *Biochim. Biophys. Acta* 592, 13–27. doi: 10.1016/0005-2728(80)90110-3

Weits, D. A., Giuntoli, B., Kosmacz, M., Parlanti, S., Hubberten, H. M., Riegler, H., et al. (2014). Plant cysteine oxidases control the oxygen-dependent branch of the N-end-rule pathway. *Nat. Commun.* 5:3425. doi: 10.1038/ncomms4425

Wheeler, M. C., Tronconi, M. A., Drincovich, M. F., Andreo, C. S., Flugge, U. I., and Maurino, V. G. (2005). A comprehensive analysis of the NADP-malic enzyme gene family of *Arabidopsis*. *Plant Physiol.* 139, 39–51. doi: 10.1104/pp.105.065953

Xia, J. H., Saglio, P., and Roberts, J. K. M. (1995). Nucleotide levels do not critically determine survival of maize root tips acclimated to a low-oxygen environment. *Plant Physiol.* 108, 589–595. doi: 10.1104/pp.108.2.589

Conflict of Interest Statement: The authors declare that the research was conducted in the absence of any commercial or financial relationships that could be construed as a potential conflict of interest.